C.5 65766

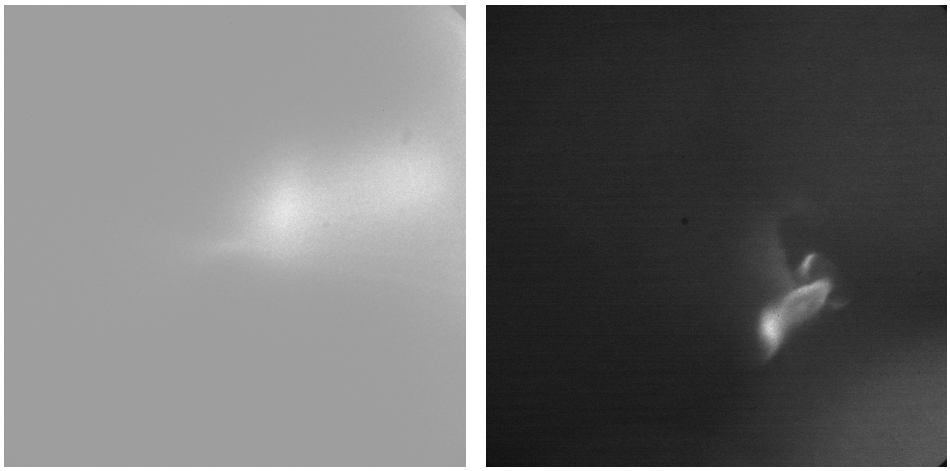

Figure C.25: GOI and TPDI of 65766. GOI (left), 20 ns after drive, and TPDI (right), 25 ns after drive, images from 65766. Single jet traveling toward the viewer in TIM 6. This was the first shot of the day that was traveling towards TIM 6. Here you can see the jet, the ring of the hole in the block from which it's emerging, and the faint glow of the laser-hit side in the background.

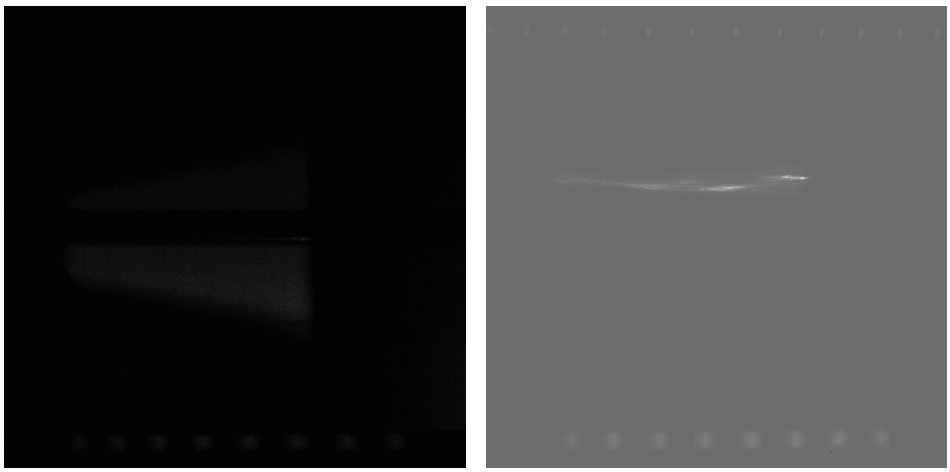

Figure C.26: Thomson spectra for 65766. EPW (left) and IAW (right) images from 65766. Probe beam fired from 15 to 18 ns.

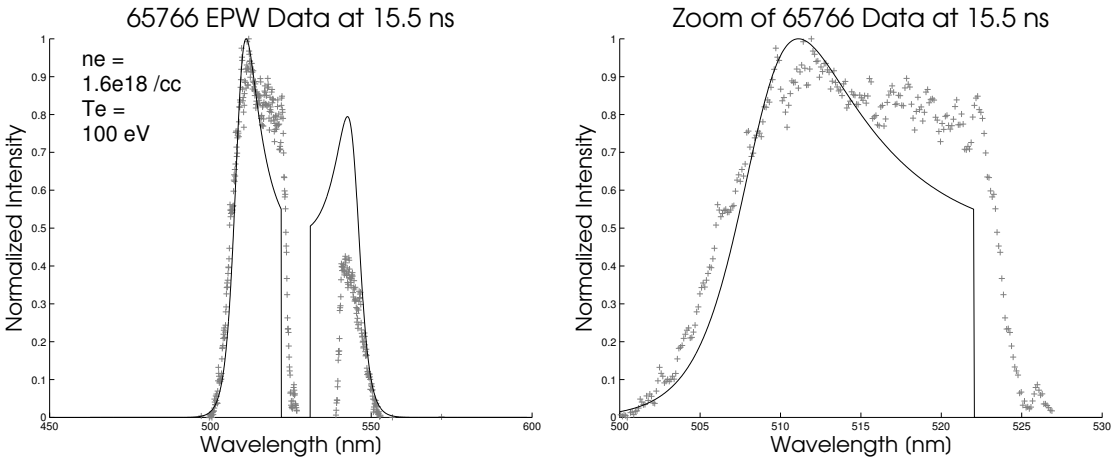

Figure C.27: 65766 EPW data at 15.5 ns

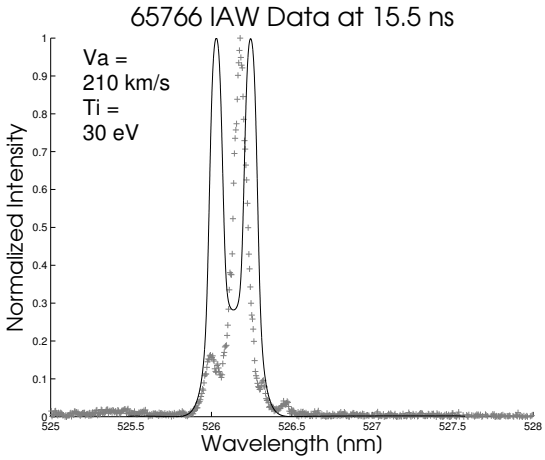

Figure C.28: 65766 IAW data at 15.5 ns

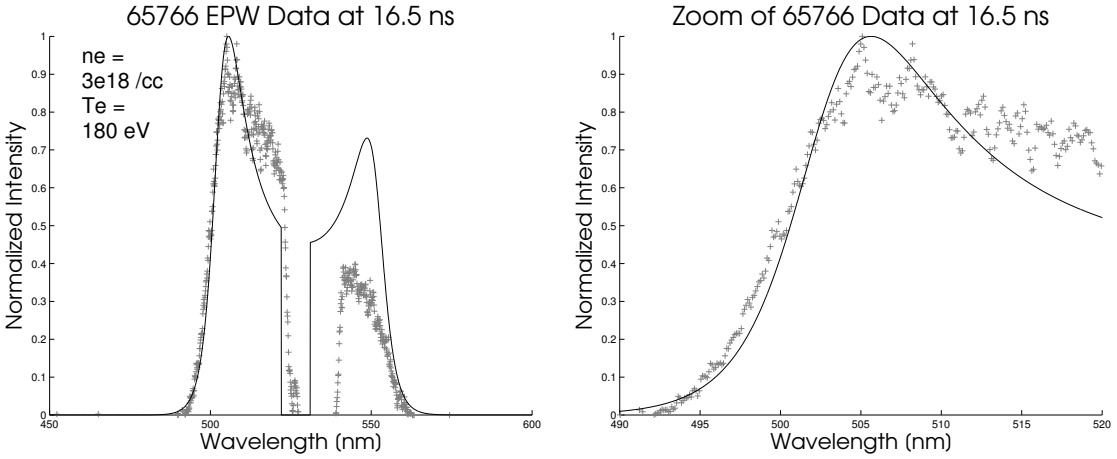

Figure C.29: 65766 EPW data at 16.5 ns

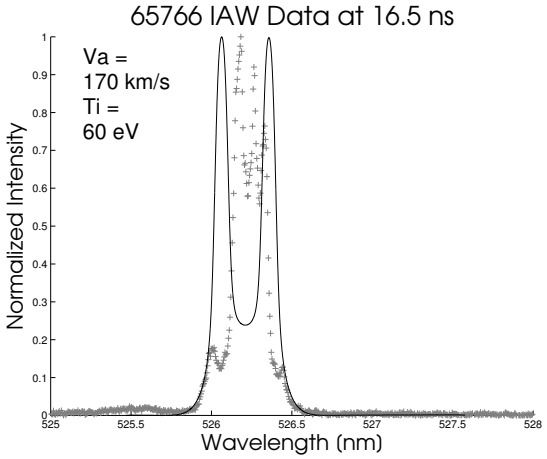

Figure C.30: 65766 IAW data at 16.5 ns

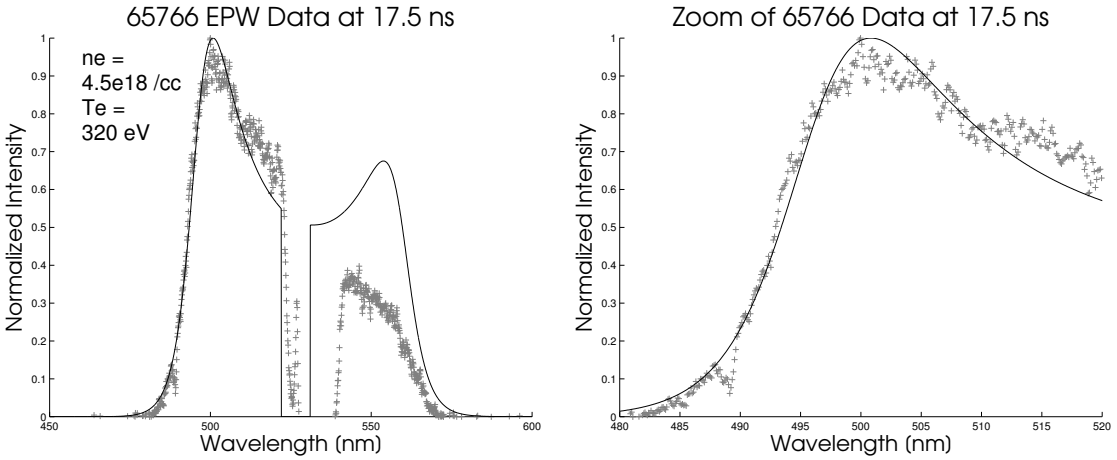

Figure C.31: 65766 EPW data at 17.5 ns

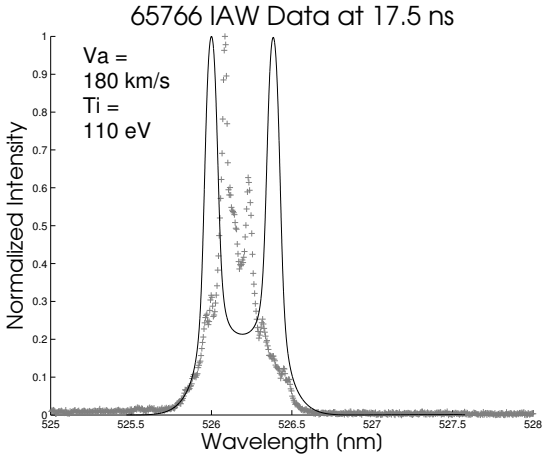

Figure C.32: 65766 EPW data at 17.5 ns

C.6 65767

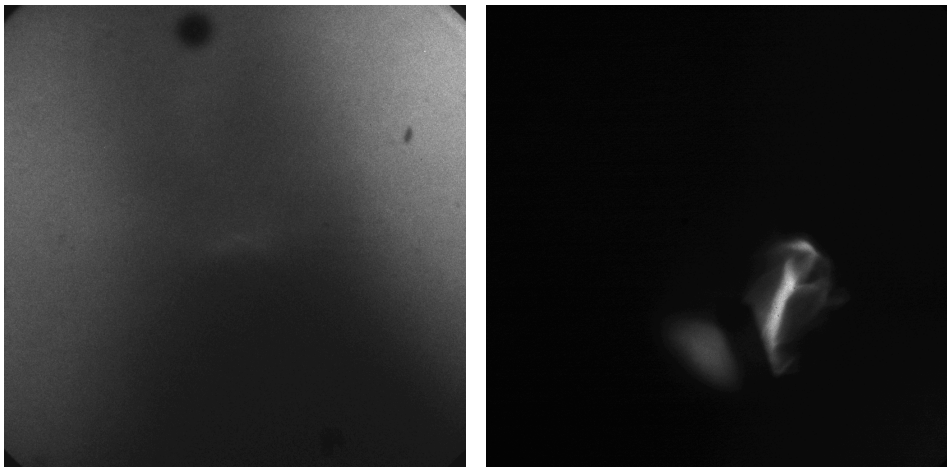

Figure C.33: GOI and TPDI of 65767. GOI (left), 20 ns after drive, and TPDI (right), 25 ns after drive, images from 65767. This was the first colliding jet shot of the day. Compare this TPDI to 65766 (jet coming towards the viewer) and 65764/65765 (jet going away from the viewer). In the foreground we see the glow of the laser-hit side of the near target. Behind that target we see one jet—the jet moving away from the viewer—emerging. In the background we see the other jet—the one coming towards the viewer—coming out. The bright spot in the middle is the collision.

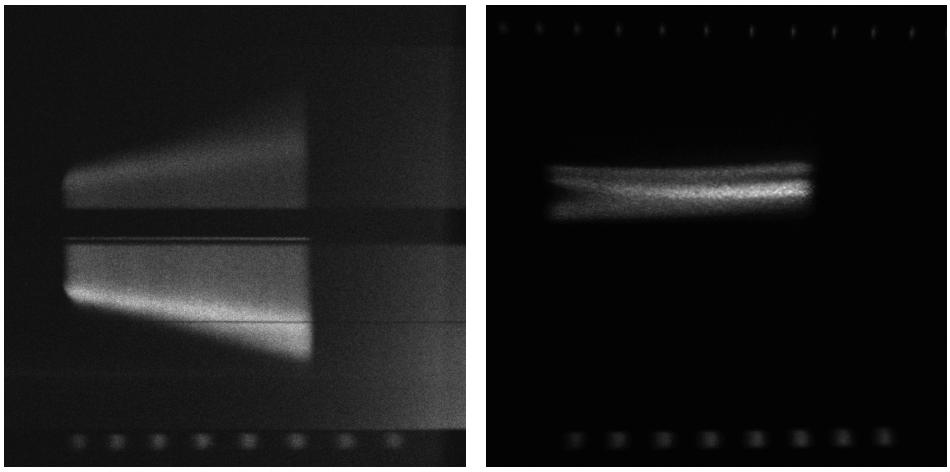

Figure C.34: Thomson spectra of 65767. EPW (left) and IAW (right) images from 65767. Probe beam fired from 15 to 18 ns. The IAW data from this shot and the other colliding jet shot are peculiar and have been relegated to their own section.

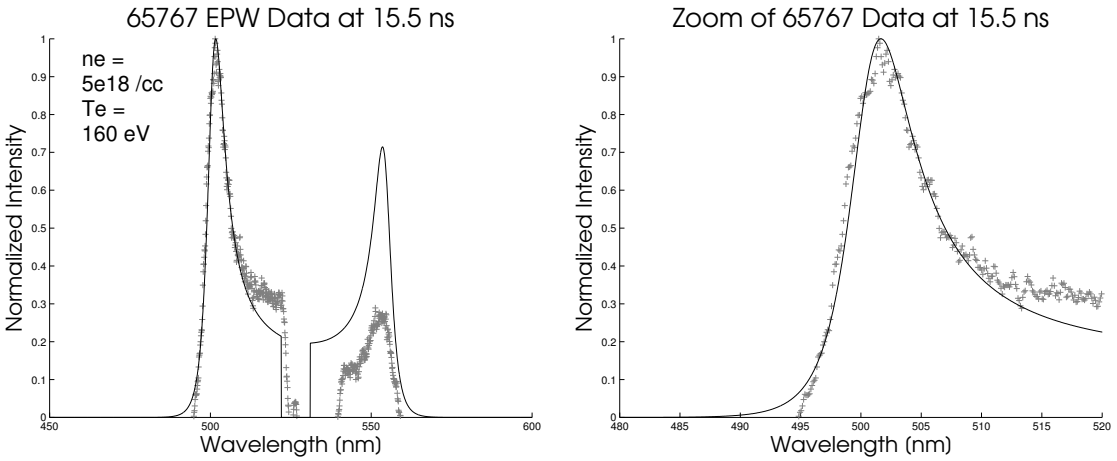

Figure C.35: 65767 EPW data at 15.5 ns

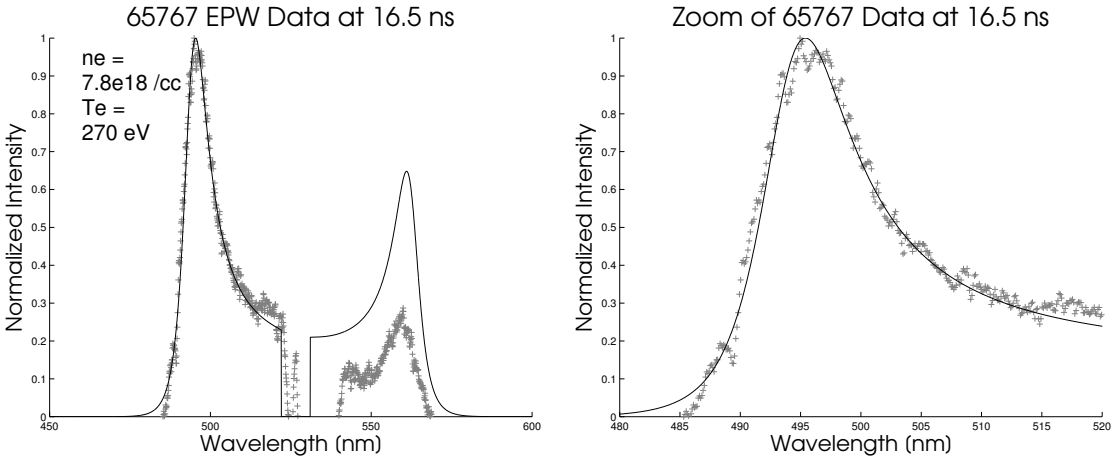

Figure C.36: 65767 EPW data at 16.5 ns

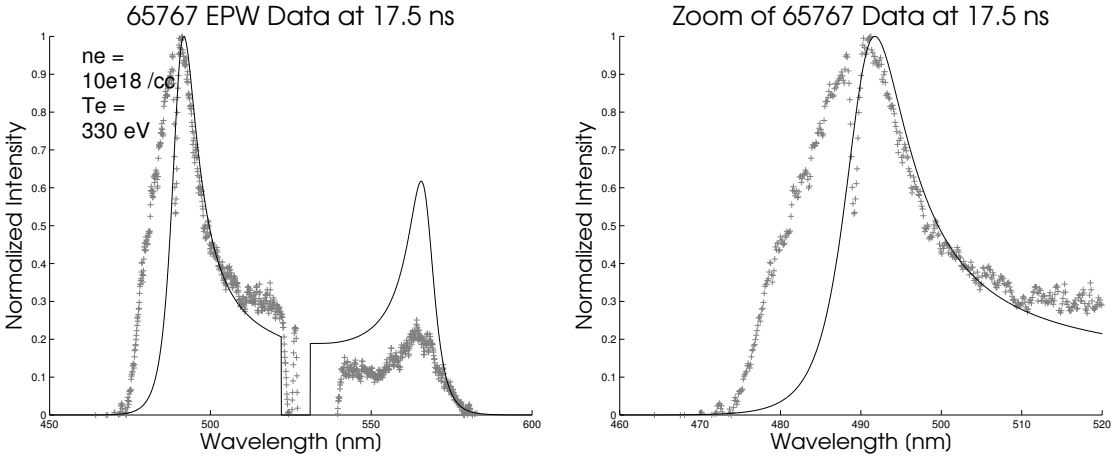

Figure C.37: 65767 EPW data at 17.5 ns

C.7 65769

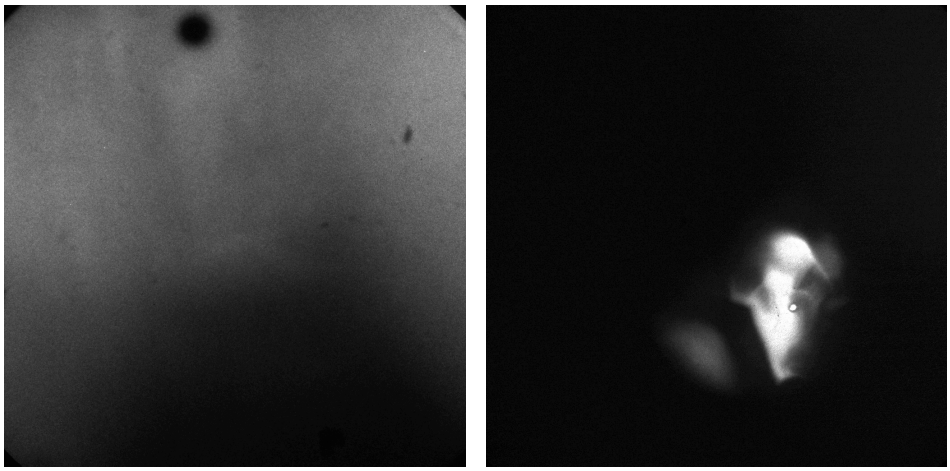

Figure C.38: GOI and TPDI of 65769. GOI (left), 25 ns after drive, and TPDI (right), 30 ns after drive, images from 65769. Colliding jet shot. The bright areas from the previous shot (at 25 ns) have grown.

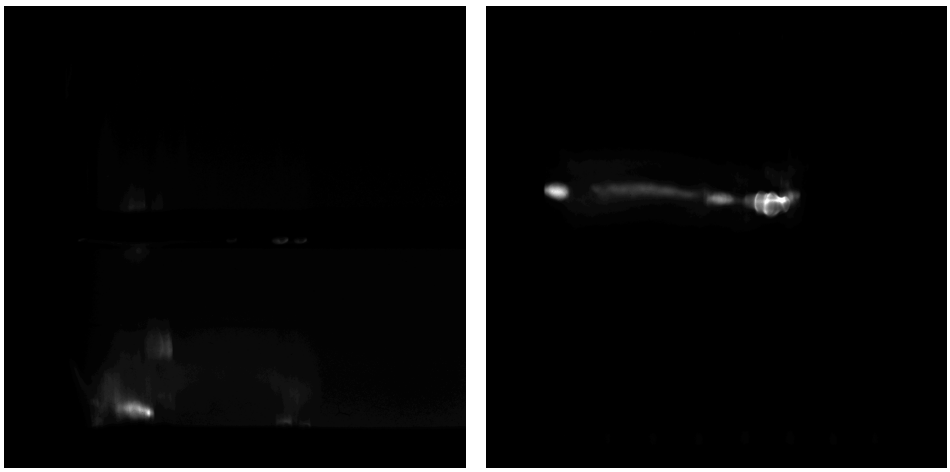

Figure C.39: Thomson spectra of 65769. EPW (left) and IAW (right) images from 65769. Probe beam fired from 20 to 23 ns. The electron density was too high and the plasma reflected the probe beam; no usable data were obtained.

C.8 65770

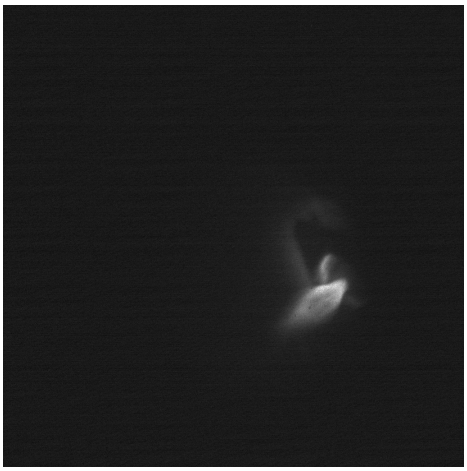

Figure C.40: GOI and TPDI of 65770. TPDI (right), 20 ns after drive, images from 65770. Single jet moving away from the viewer in TIM 6. No GOI image was obtained for this shot.

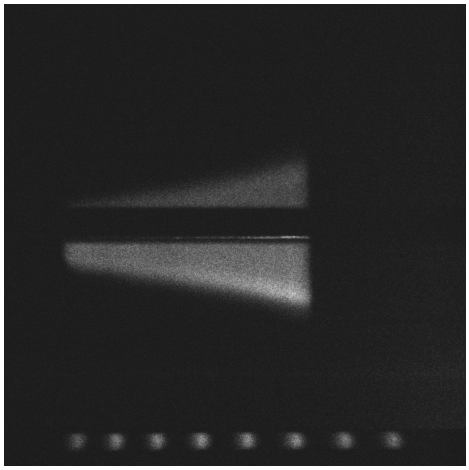

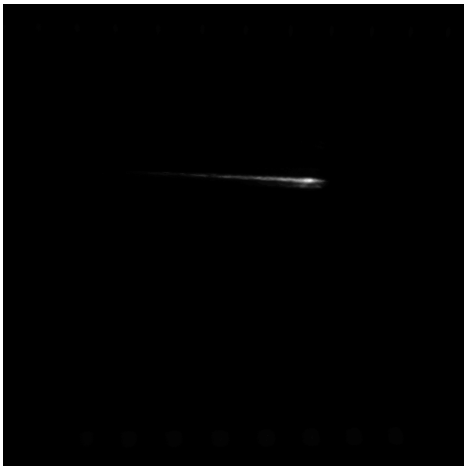

Figure C.41: Thomson spectra of 65770. EPW (left) and IAW (right) images from 65770. Probe beam fired from 12 to 15 ns.

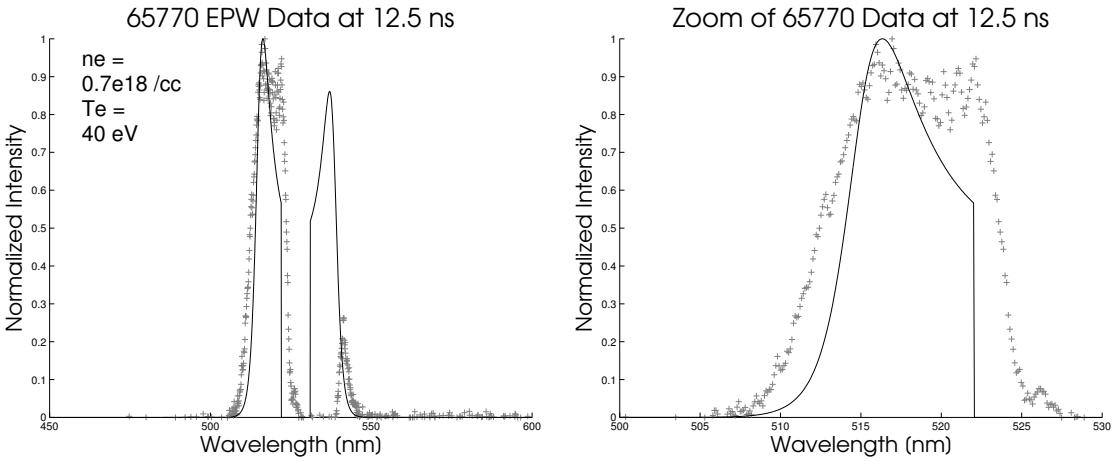

Figure C.42: 65770 EPW data at 12.5 ns

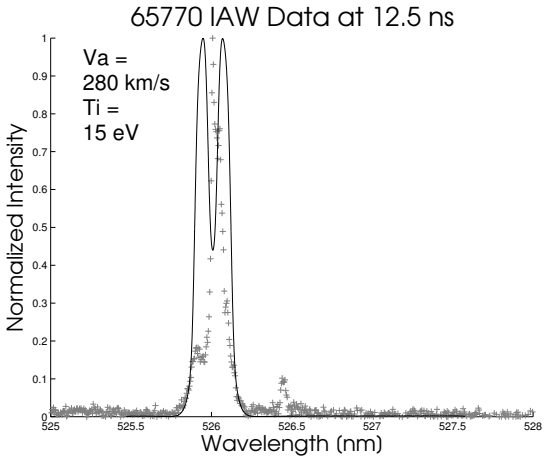

Figure C.43: 65770 IAW data at 12.5 ns

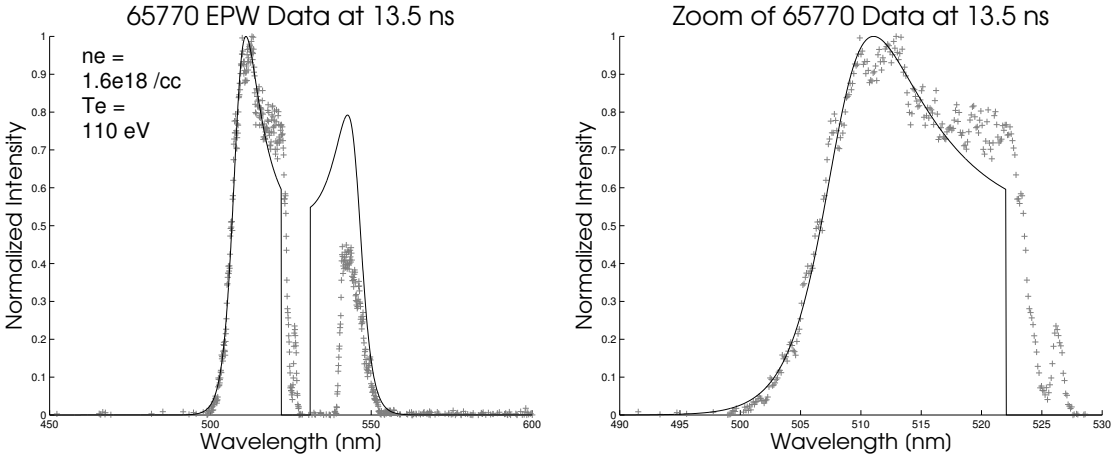

Figure C.44: 65770 EPW data at 13.5 ns

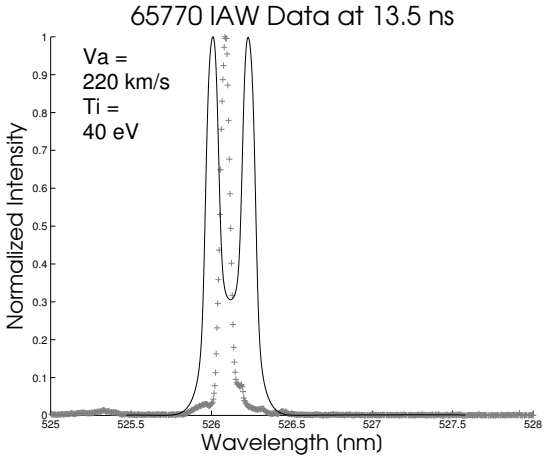

Figure C.45: 65770 IAW data at 13.5 ns

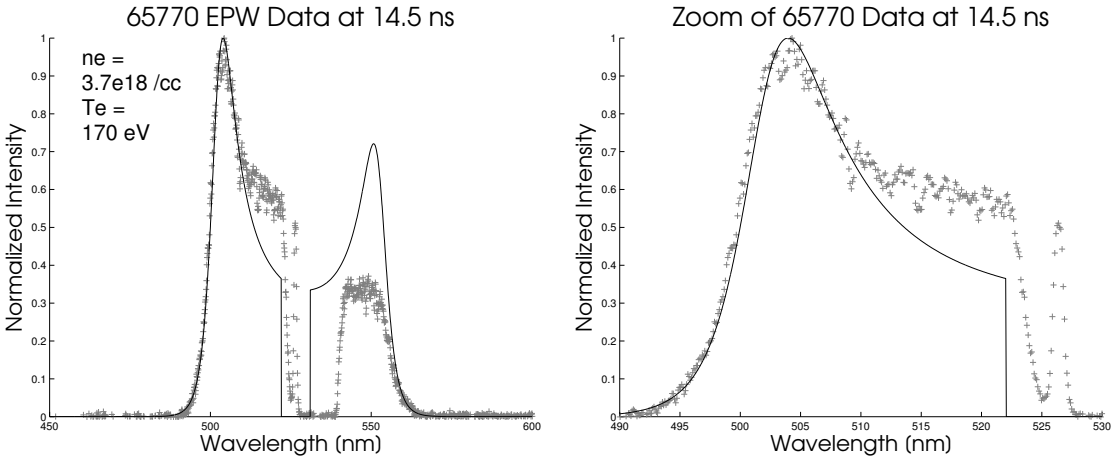

Figure C.46: 65770 EPW data at 14.5 ns

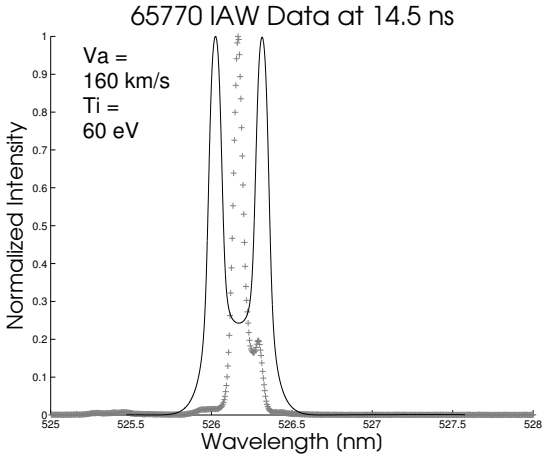

Figure C.47: 65770 EPW data at 14.5 ns

C.9 65774

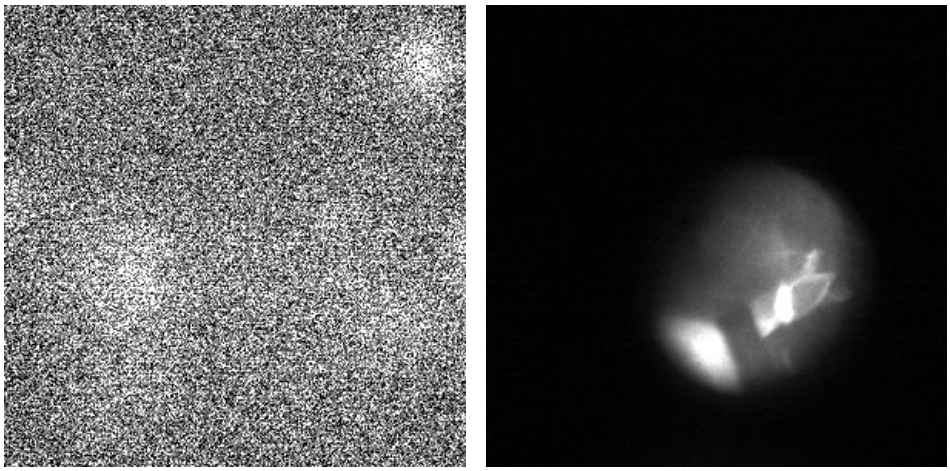

Figure C.48: GOI and TPDI of 65774. GOI (left), 30 ns after drive, and TPDI (right), 20 ns after drive, images from 65774. Colliding jets shot. Compared to the later colliding shots (65767 at 25 ns and 65769 at 30 ns) this TPDI image is clearer; the hott collision zone regions have yet to get really bright.

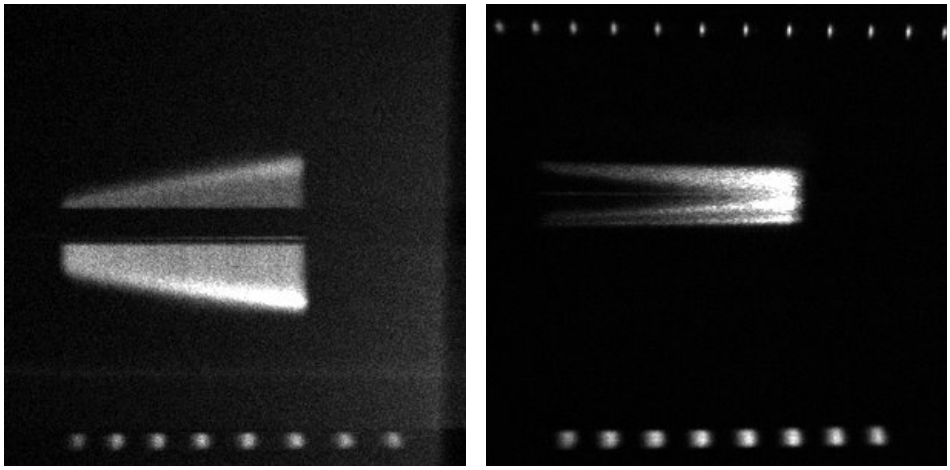

Figure C.49: Thomson spectra of 65774. EPW (left) and IAW (right) images from 65774. Probe beam fired from 12 to 15 ns. As with 65767, the IAW data are peculiar and have been relegated to their own section.

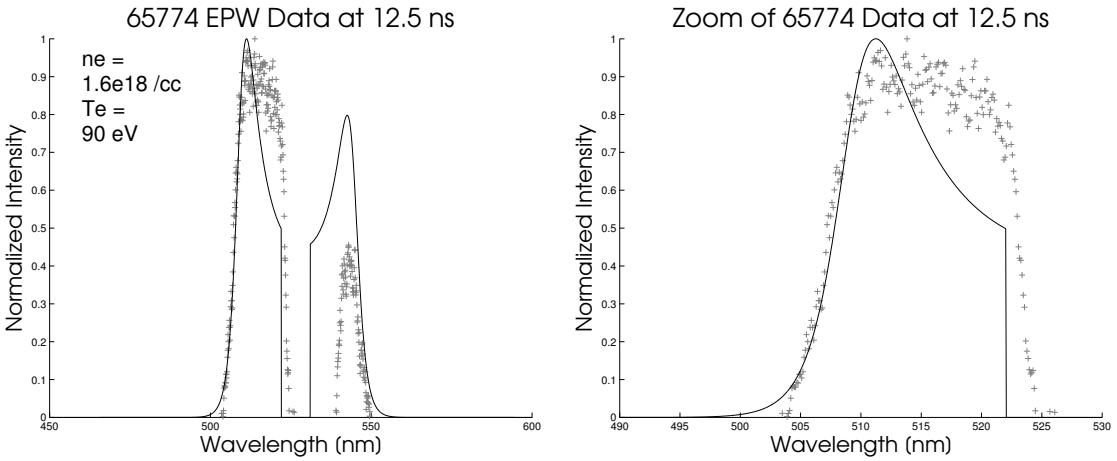

Figure C.50: 65774 EPW data at 12.5 ns

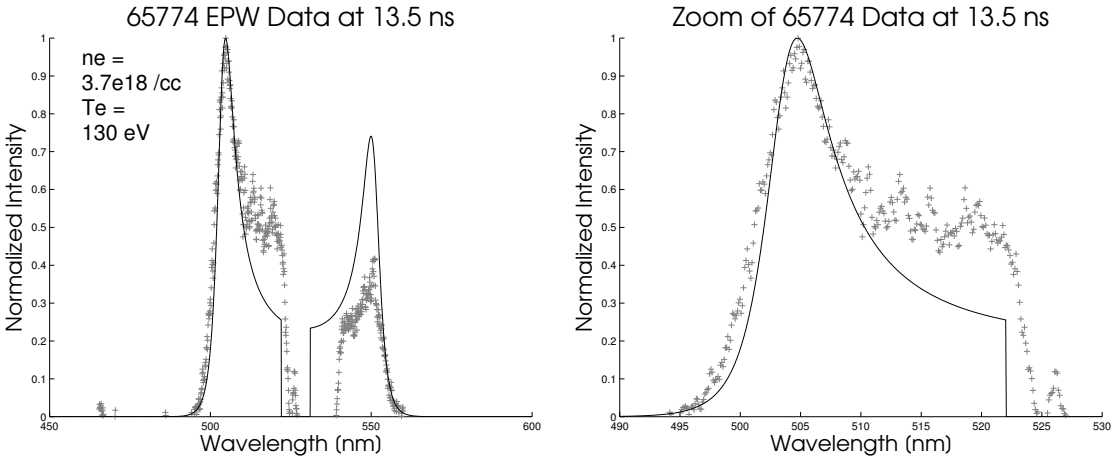

Figure C.51: 65774 EPW data at 13.5 ns

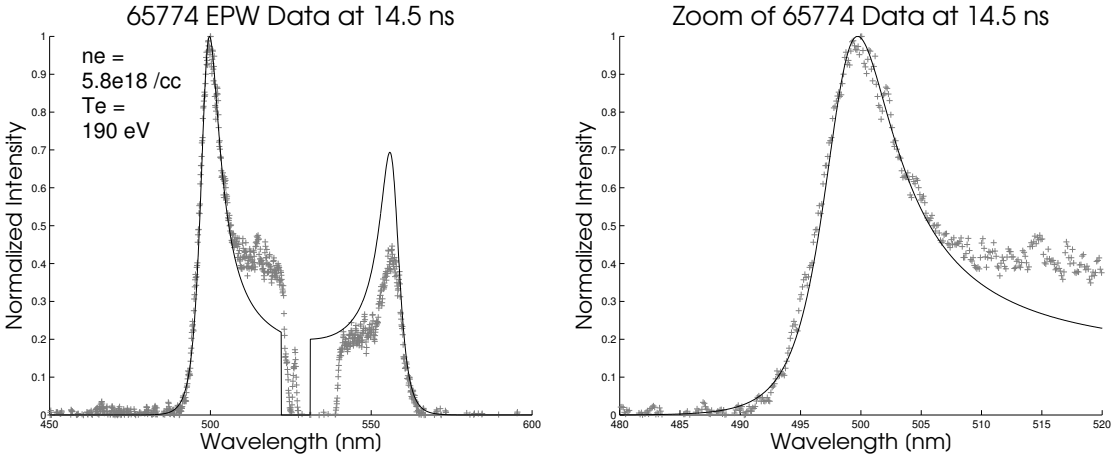

Figure C.52: 65774 EPW data at 14.5 ns

C.10 Colliding Jet Shot IAW Data

The colliding jet IAW data show signs of interpenetrating flows moving at different velocities.

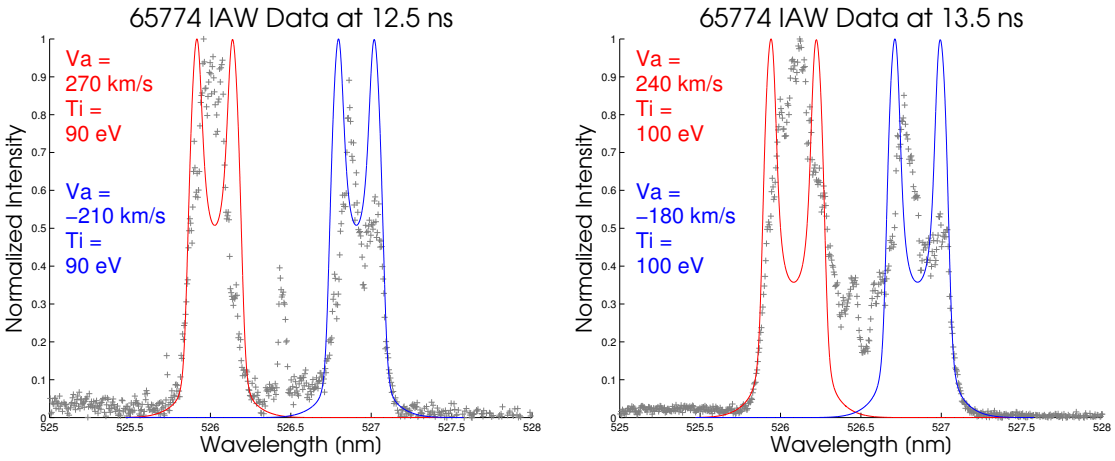

Figure C.53: 65774 IAW data at 12.5 and 13.5 ns

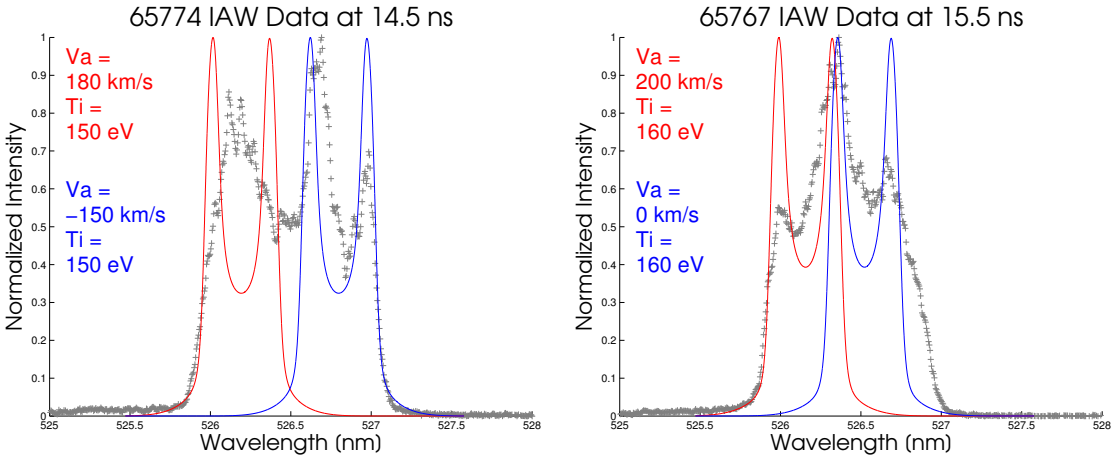

Figure C.54: 65774 IAW data at 14.5 and 65767 IAW data at 15.5 ns

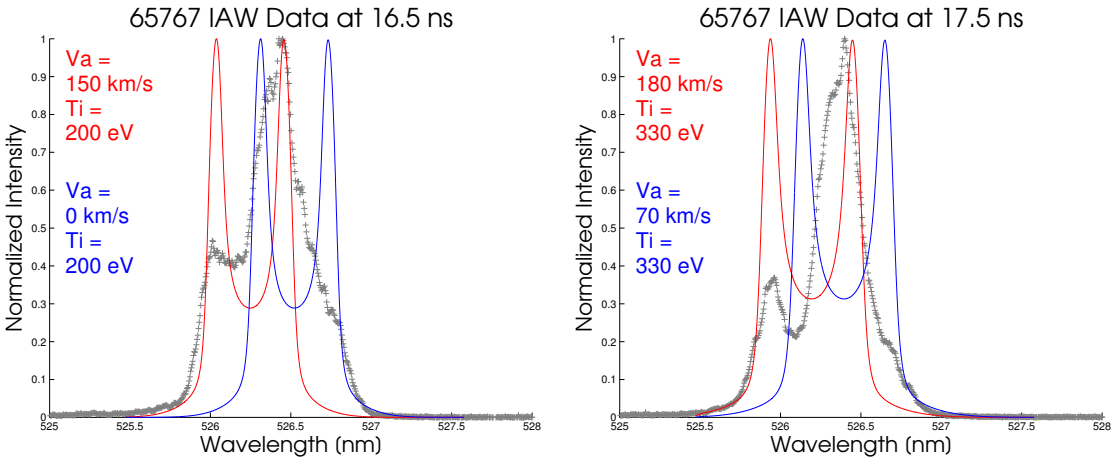

Figure C.55: 65767 IAW data at 16.5 and 17.5 ns

APPENDIX D

Data from August 2013

D.1 70672

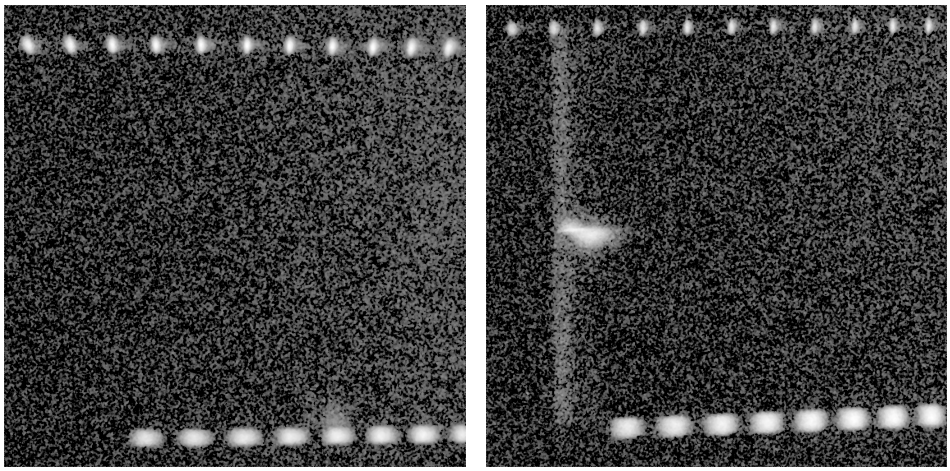

Figure D.1: Thomson data for Shot 70672; EPW (left) and IAW (right). Jet B was launched 18 ns before Thomson probe; probe length was 1 ns. The probe beam was fired much too early; later shots indicate that it needed to be around 40 ns.

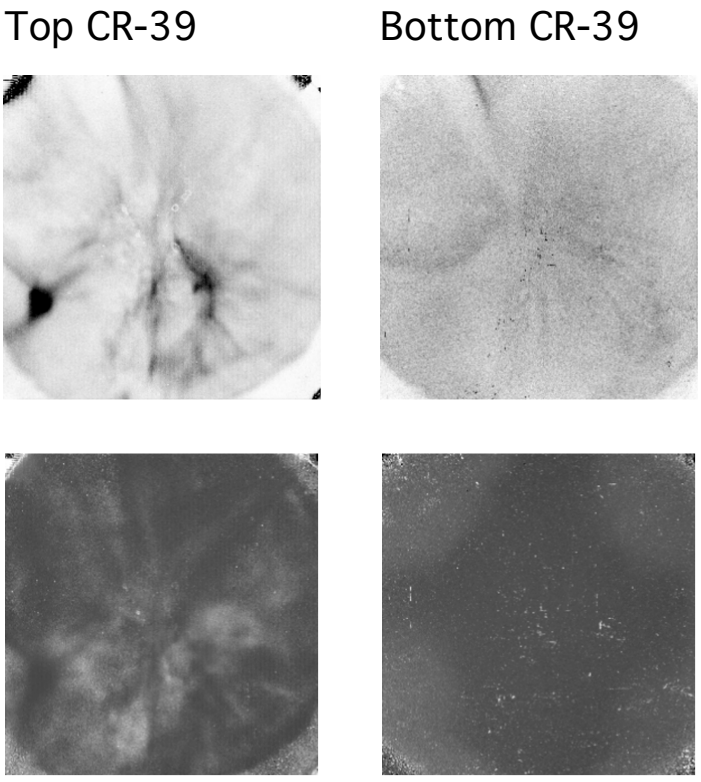

Figure D.2: Proton radiography data for Shot 70672. Backlighter fired 20 ns after drive beams. MIFEDS charged for this shot. No evidence of jets is seen, probably because the data were collected too early.

D.2 70673

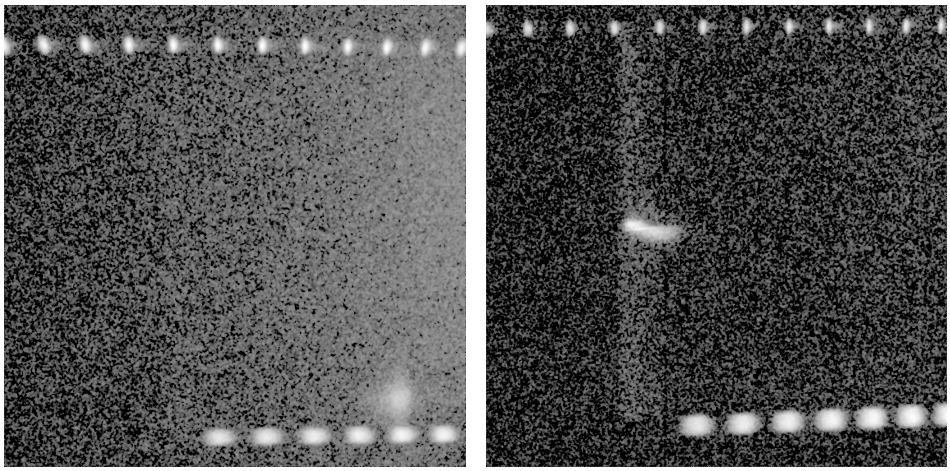

Figure D.3: Thomson data for Shot 70673; EPW (left) and IAW (right). Jet B was launched 25 ns before Thomson probe; probe length was 1 ns. No good data was obtained, probe was still timed too early.

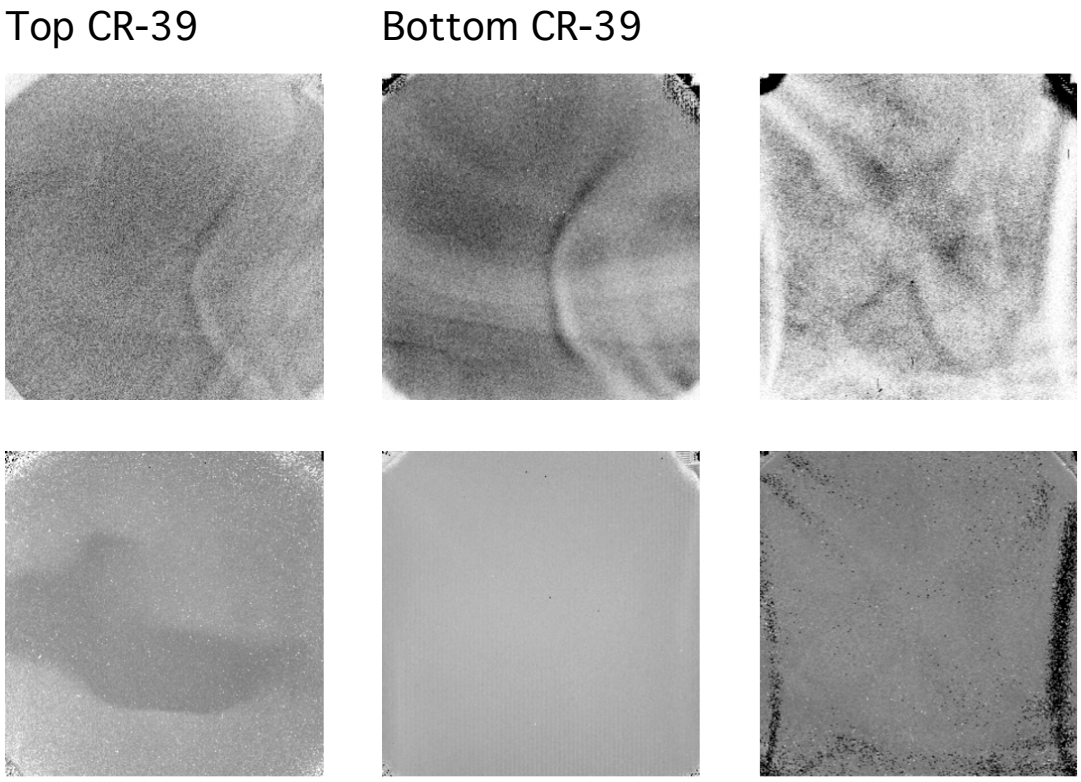

Figure D.4: Proton radiography data for Shot 70673. Backlighter fired 27 ns after drive beams. MIFEDS did not charge for this shot. A faint "bubble" from the jet emerging into the field of view is visible.

D.3 70674

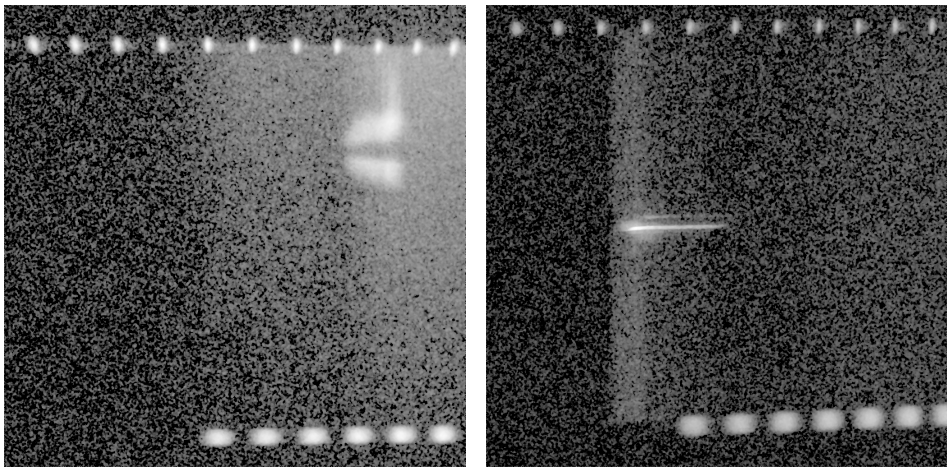

Figure D.5: Thomson data for Shot 70674; EPW (left) and IAW (right). Jet C was launched 30 ns before Thomson probe; probe length was 1 ns. Good data obtained.

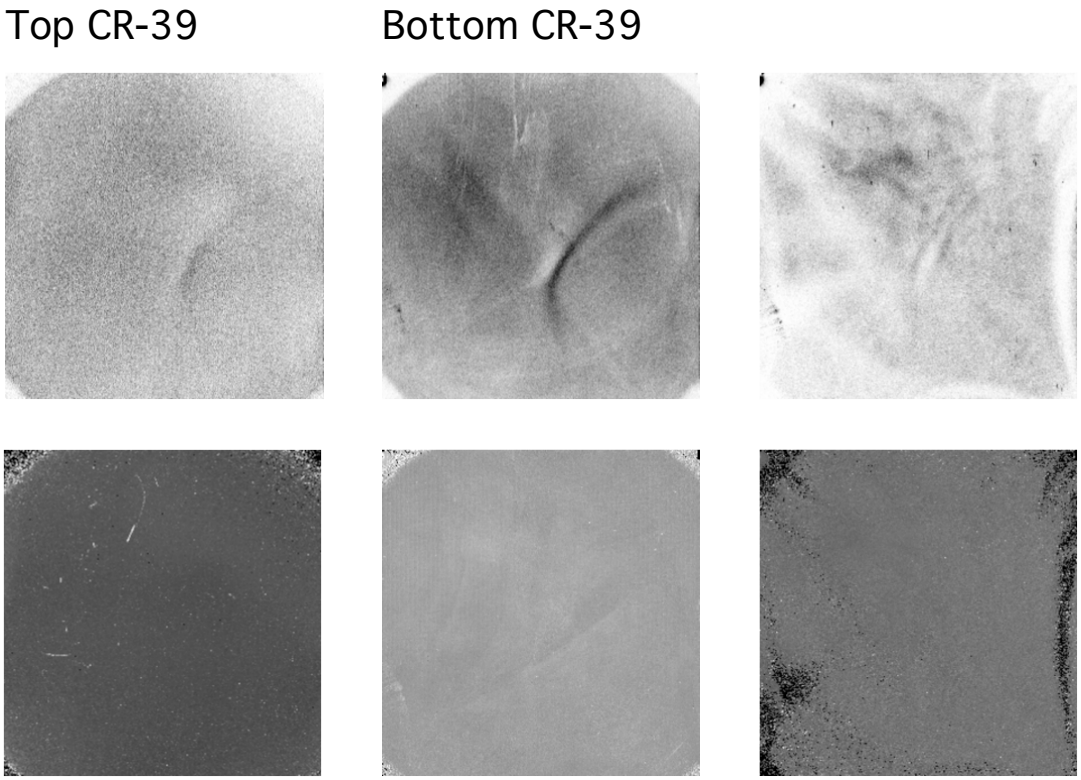

Figure D.6: Proton radiography data for Shot 70674. Backlighter fired 32 ns after drive beams. MIFEDS did not charge for this shot. Oddly, this bubble is oriented the same way it was for Shot 70673, even though Jet B was fired that shot and Jet C was fired for this shot.

D.4 70678

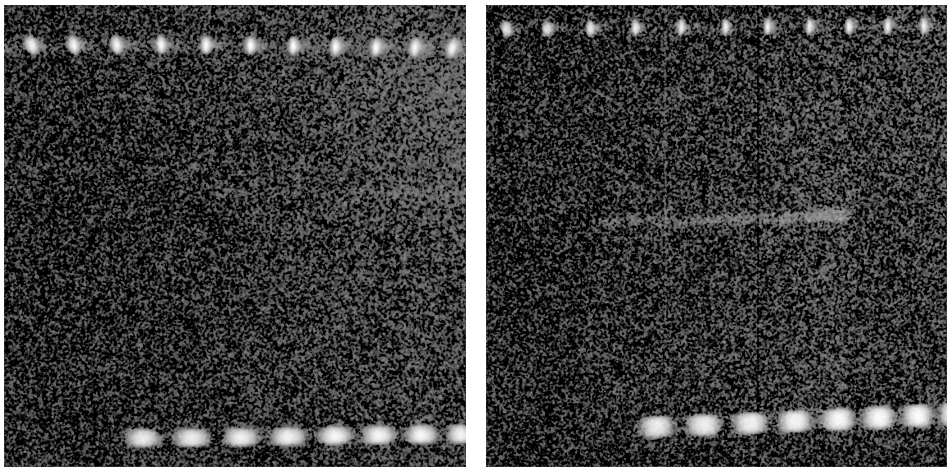

Figure D.7: Thomson data for Shot 70678; EPW (left) and IAW (right). Jet B was launched 30 ns before Thomson probe; probe length was increased 3 ns and no proton backlighter was used. This configuration did not use MIFEDS. Problems with the EPW data persist, but the IAW data appears clear over the 3-ns pulse.

D.5 70679

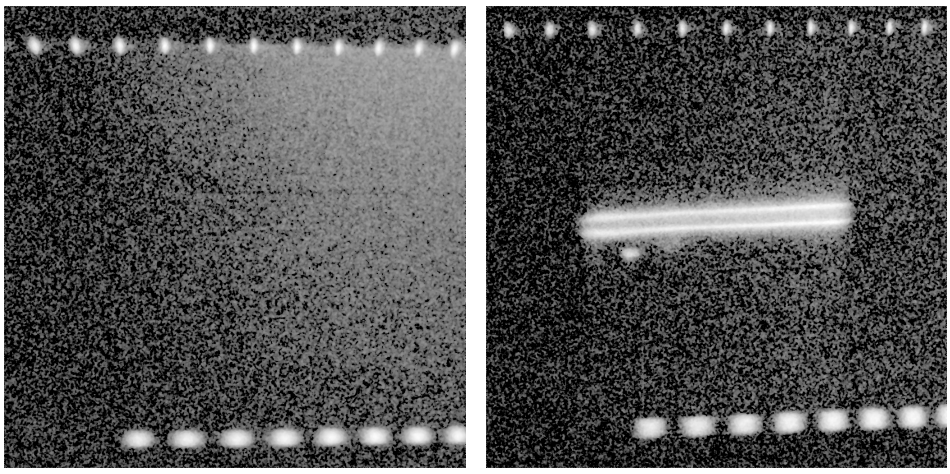

Figure D.8: Thomson data for Shot 70679; EPW (left) and IAW (right). Jet B was launched 40 ns before Thomson probe; probe length remained at 3 ns and no proton backlighter was used. This configuration did not use MIFEDS. This is some of the best IAW data obtained for this shot day.

D.6 70680

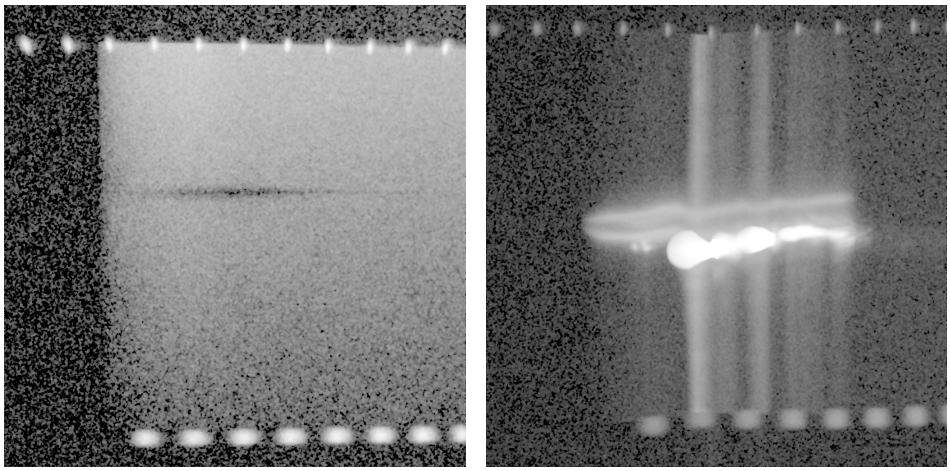

Figure D.9: Thomson data for Shot 70680; EPW (left) and IAW (right). Jet B was launched 50 ns before Thomson probe; probe length remained at 3 ns and no proton backlighter was used. This configuration did not use MIFEDS. Some IAW data is visible, but there is significant interference from reflected light.

D.7 70681

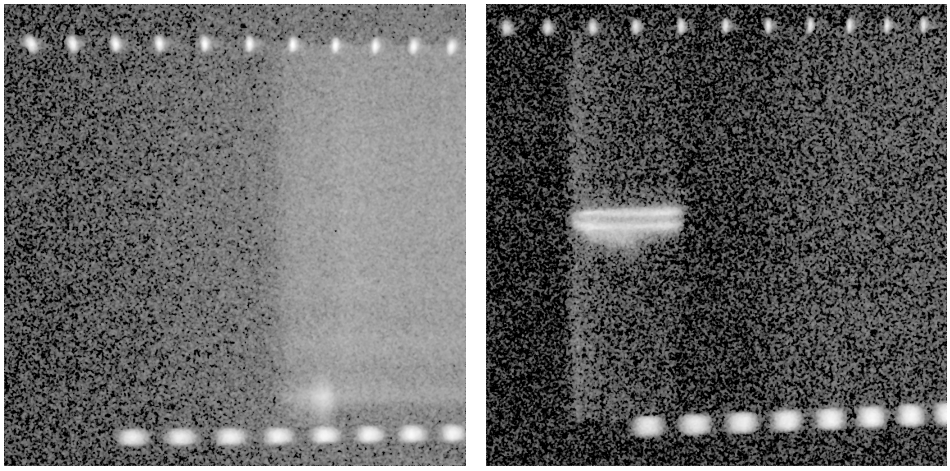

Figure D.10: Thomson data for Shot 70681; EPW (left) and IAW (right). Jet B was launched 40 ns before Thomson probe; probe length was decreased back to 1 ns. Good IAW data obtained.

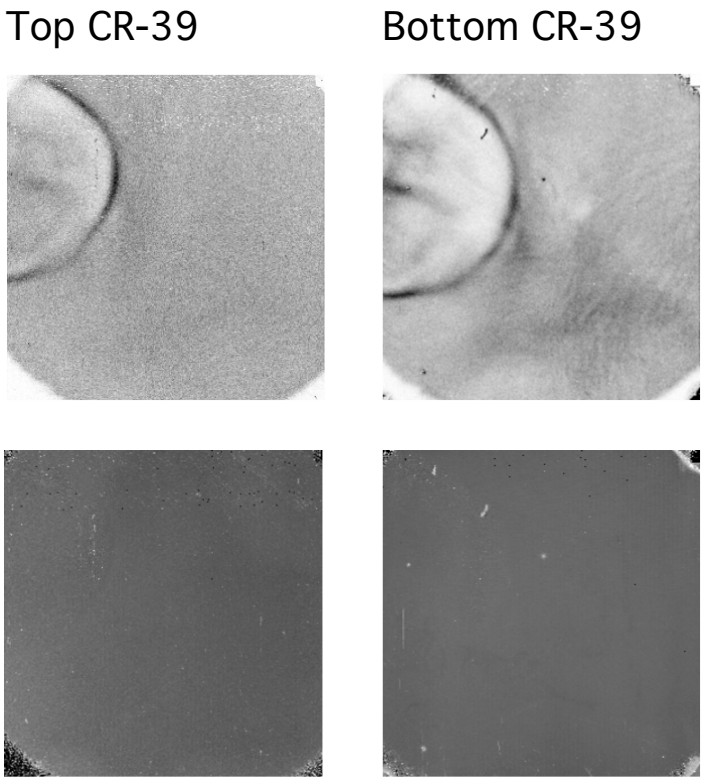

Figure D.11: Proton radiography data for Shot 70681. Backlighter fired 42 ns after drive. MIFEDS was charged for this shot, but failed. The orientation is odd–were the blocks inadvertently rotated in the developing process?

D.8 70682

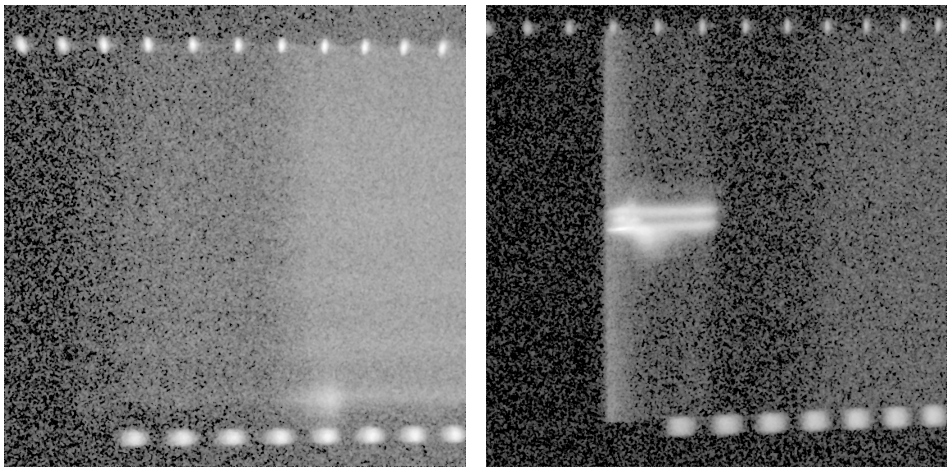

Figure D.12: Thomson data for Shot 70682; EPW (left) and IAW (right). Jet B was launched 40 ns before Thomson probe; probe length remained at 1 ns. IAW data is good.

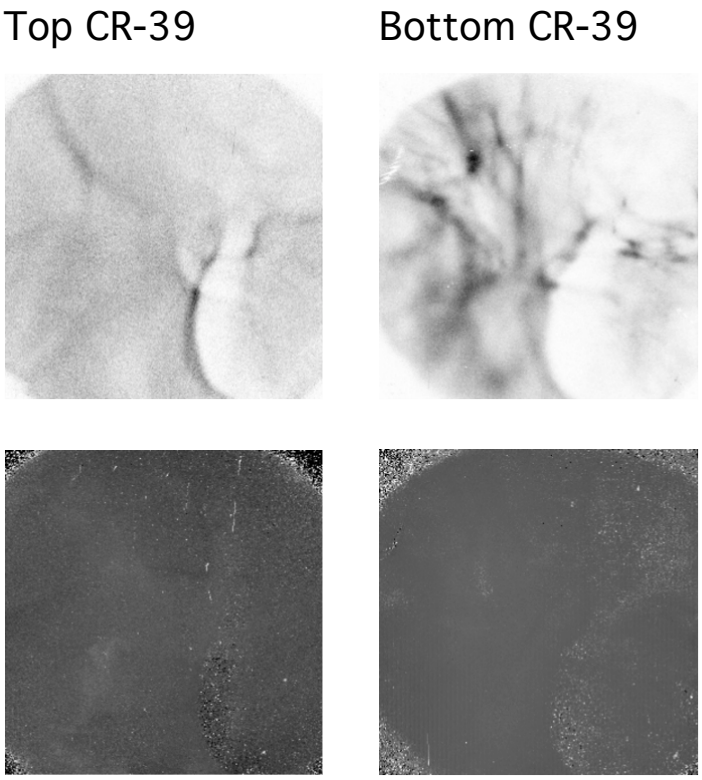

Figure D.13: Proton radiography data for Shot 70682. Backlighter fired 42 ns after drive. MIFEDS was charged for this shot. A fainter bubble is visible—the imposed field seems to interfere with the self-generated field.

D.9 70683

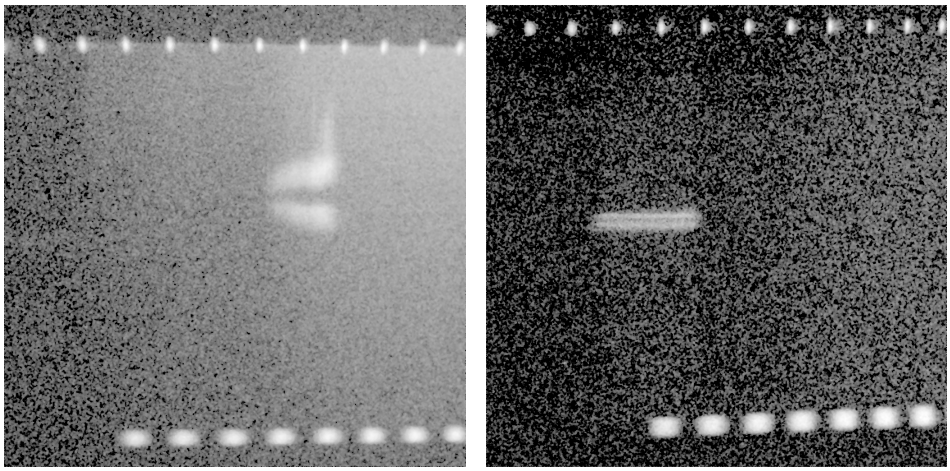

Figure D.14: Thomson data for Shot 70683; EPW (left) and IAW (right). Jets B and C were launched 40 ns before Thomson probe; probe length remained at 1 ns. Interestingly, both EPW and IAW worked on this shot.

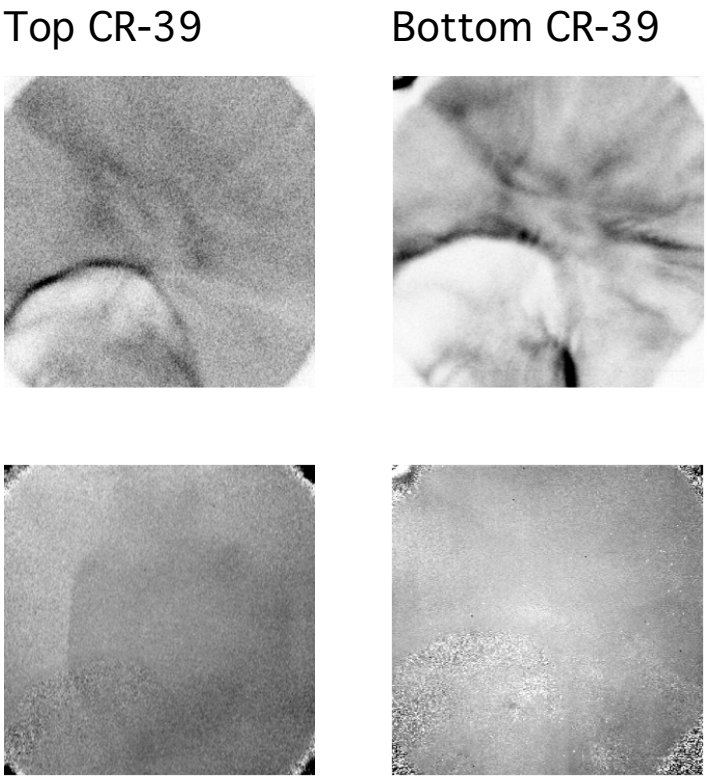

Figure D.15: Proton radiography data for Shot 70683. Backlighter fired 42 ns after drive. MIFEDS was charged for this shot. Only one bubble is visible even though two were fired.

D.10 70684

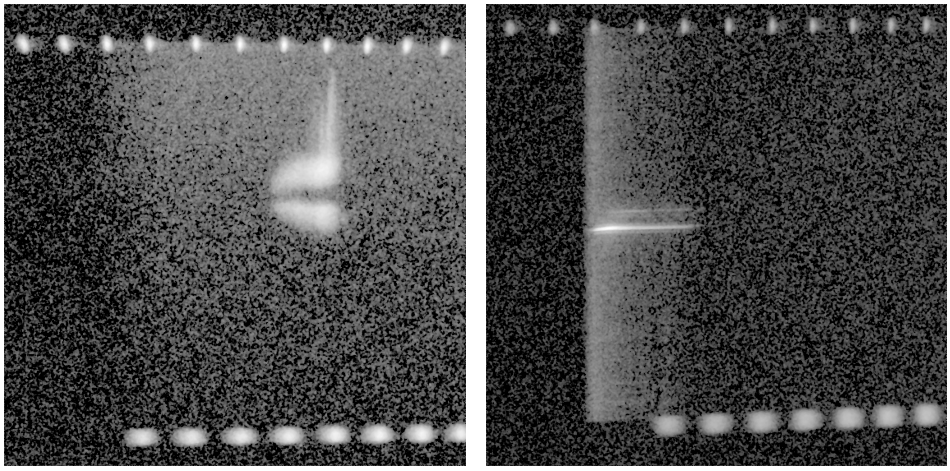

Figure D.16: Thomson data for Shot 70684; EPW (left) and IAW (right). Jets B and C were launched 40 ns before Thomson probe; probe length remained at 1 ns. Good EPW and IAW data obtained.

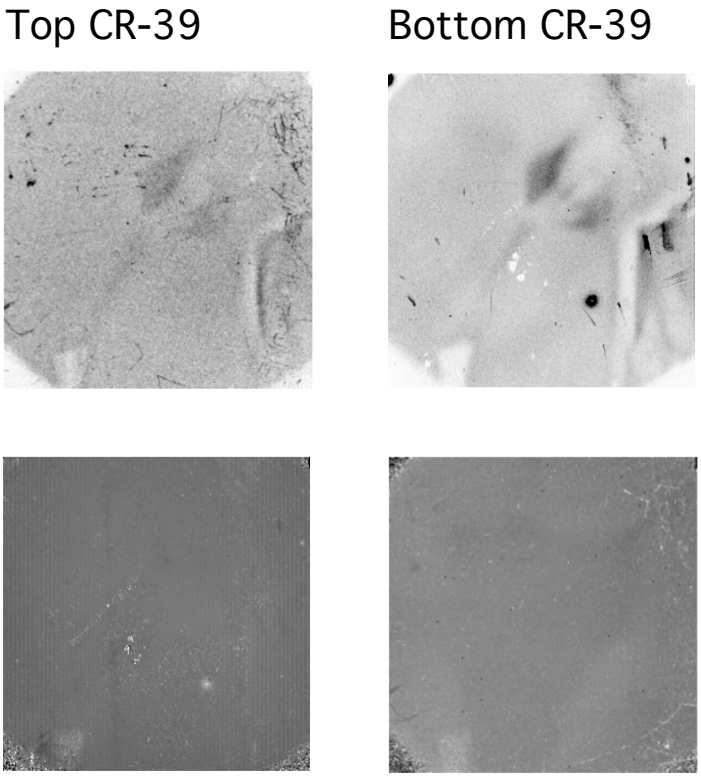

Figure D.17: Proton radiography data for Shot 70684. Backlighter fired 42 ns after drive. MIFEDS was not charged for this shot. Proton radiography appears to have failed.

APPENDIX E

Data from May 2014

E.1 73327

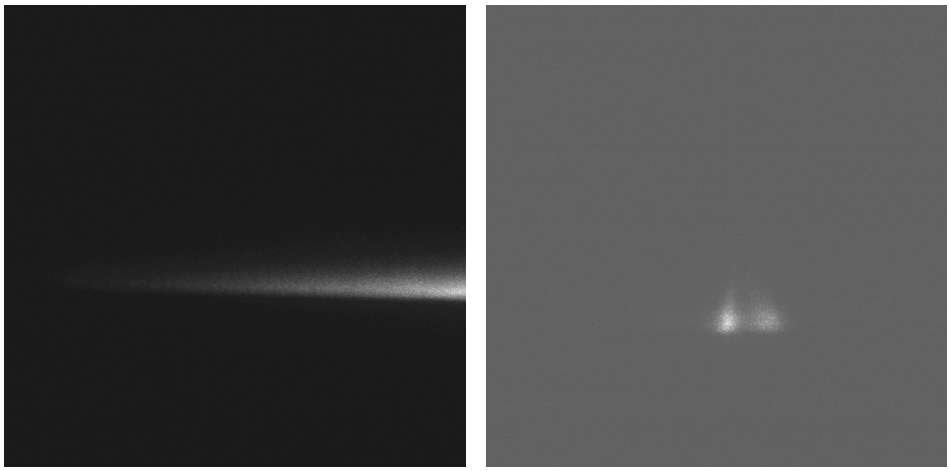

Figure E.1: Thomson data from 73327. Thomson data taken 16 ns after drive; EPW (left) and IAW (right). As seen in the IAW image, the jet is barely in range.

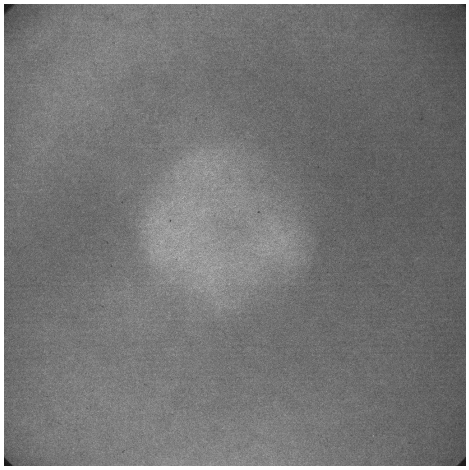

Figure E.2: Visible light data from 73327. No discernible structures observed.

E.2 73328

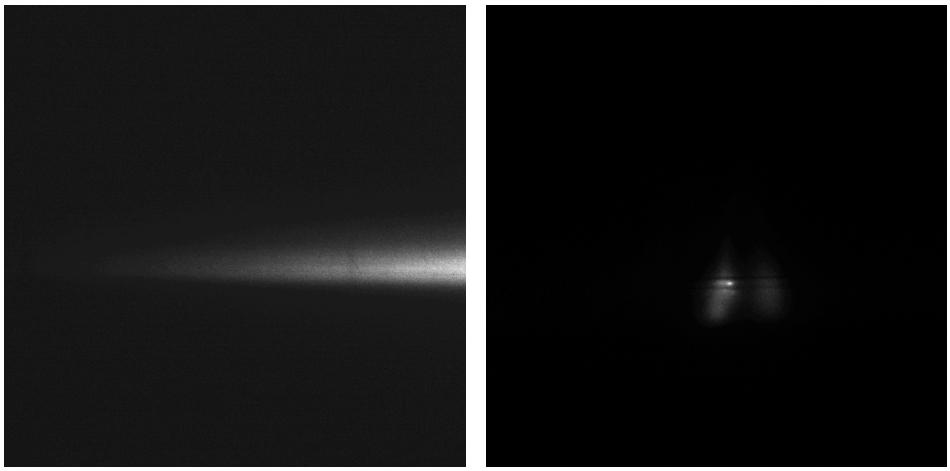

Figure E.3: Thomson data from 73328. Thomson data taken 20 ns after drive; EPW (left) and IAW (right). The timing of this shot was good.

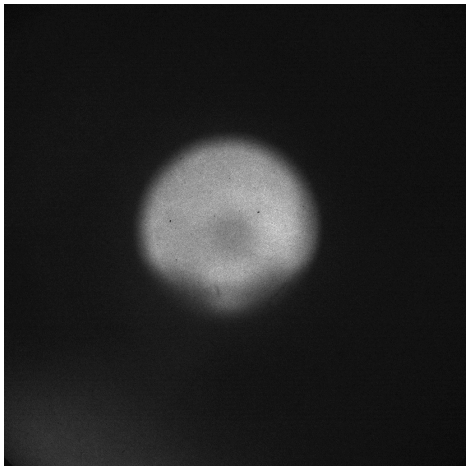

Figure E.4: Visible light data from 73328. No discernible structures observed.

E.3 73330

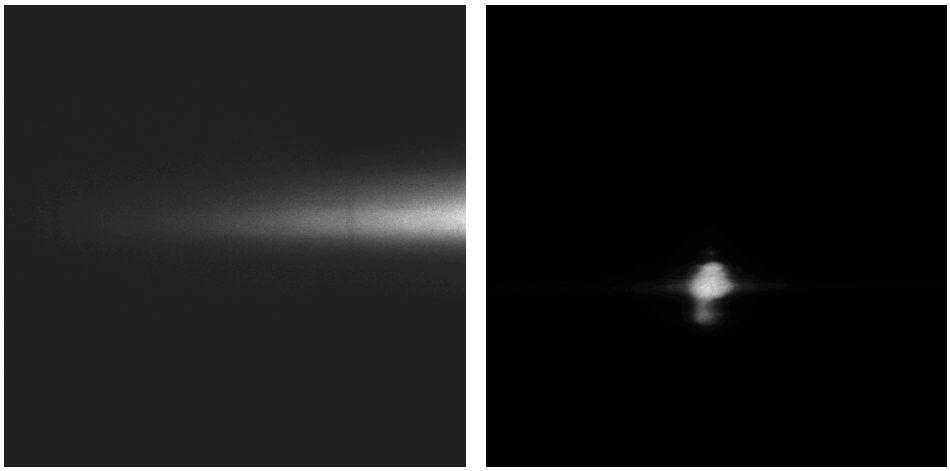

Figure E.5: Thomson data from 73330. Thomson data taken 28 ns after drive; EPW (left) and IAW (right). Densities were too high; the probe reflected off the experimental plasma.

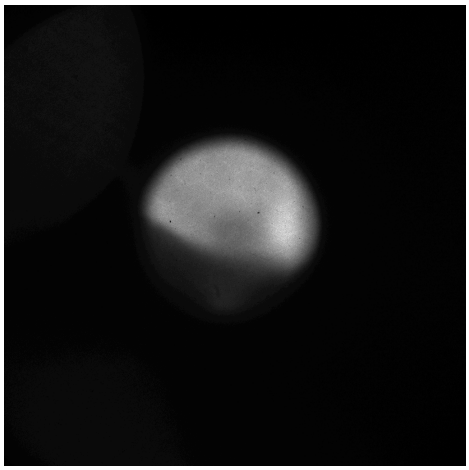

Figure E.6: Visible light data from 73330. No discernible structures observed.

E.4 73331

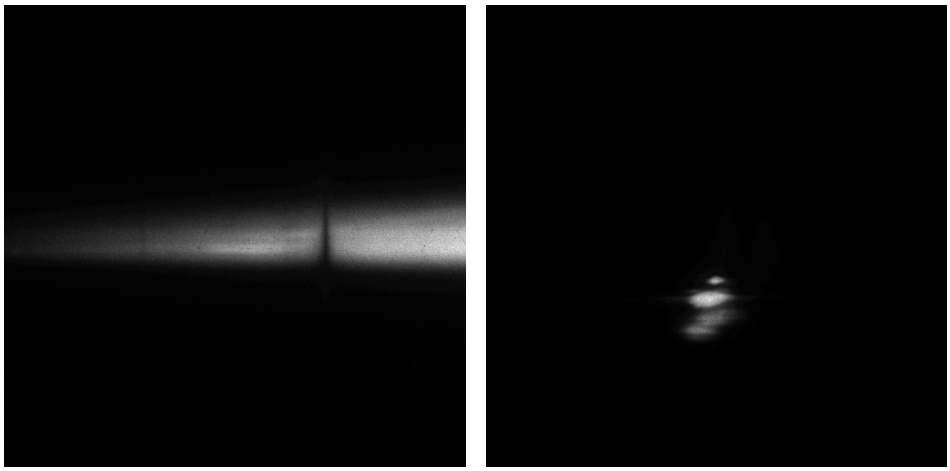

Figure E.7: Thomson data from 73331. Thomson data taken 28 ns after drive; EPW (left) and IAW (right). Densities were too high; the probe reflected off the experimental plasma.

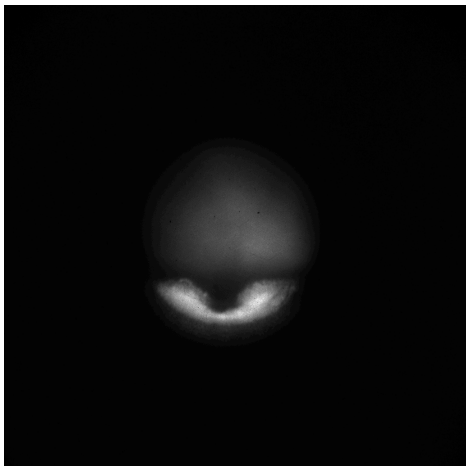

Figure E.8: Visible light data from 73331. No discernible structures observed.

E.5 73334

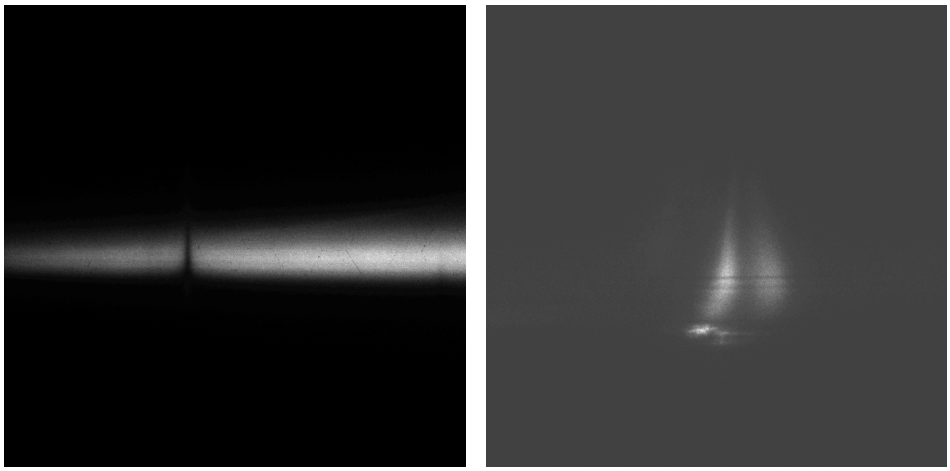

Figure E.9: Thomson data from 73334. Thomson data taken 20 ns after drive; EPW (left) and IAW (right). The timing of this shot was good.

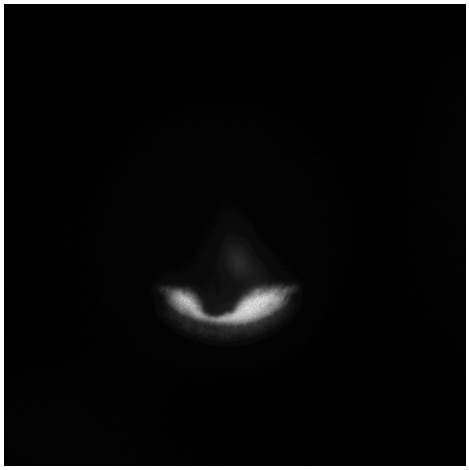

Figure E.10: Visible light data from 73334. No discernible structures observed.

E.6 73335

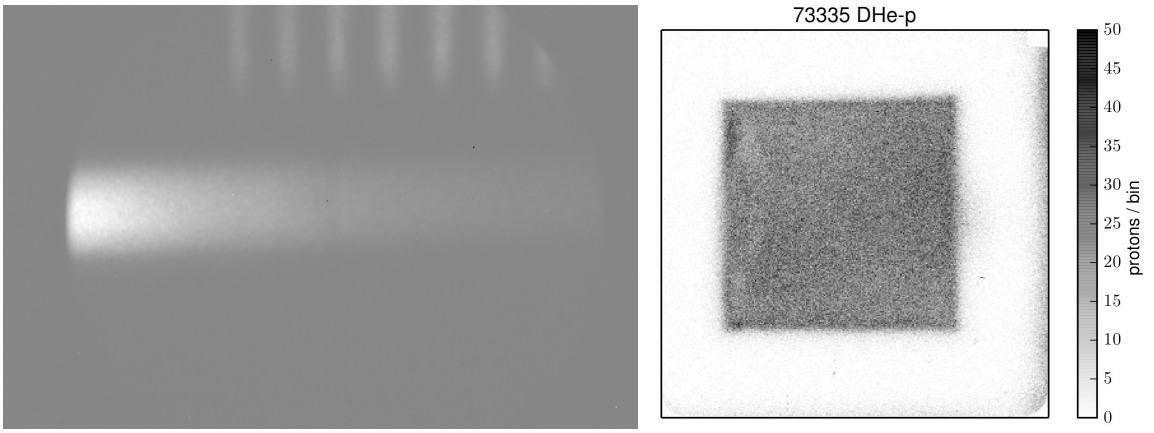

Figure E.11: Proton radiography data from 73335. Shot 73335 Particle Temporal Diagnostic (PTD) data on left; proton radiography on right. Data taken 30 ns after drive, no field imposed.

E.7 73336

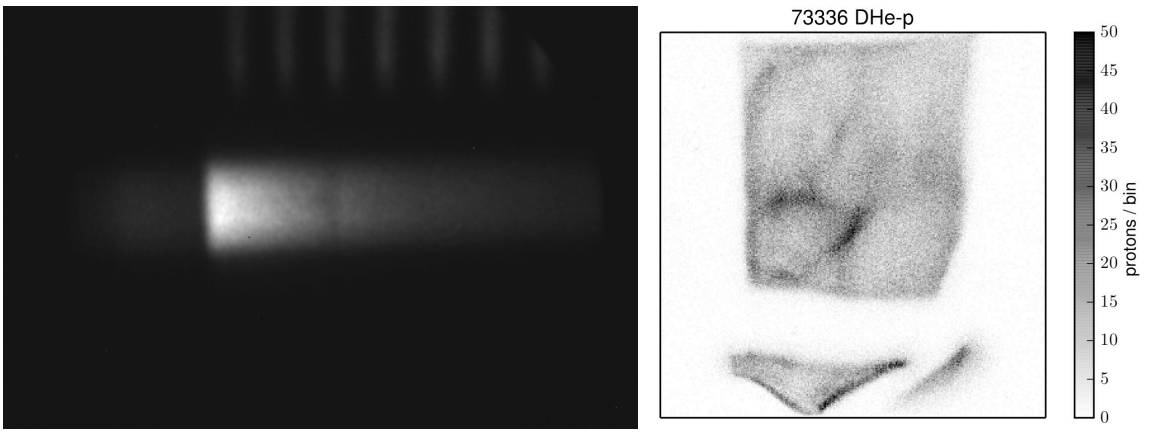

Figure E.12: Proton radiography data from 73336. Shot 73336 Particle Temporal Diagnostic (PTD) data on left; proton radiography on right. Data taken 30 ns after drive, no field imposed.

E.8 73337

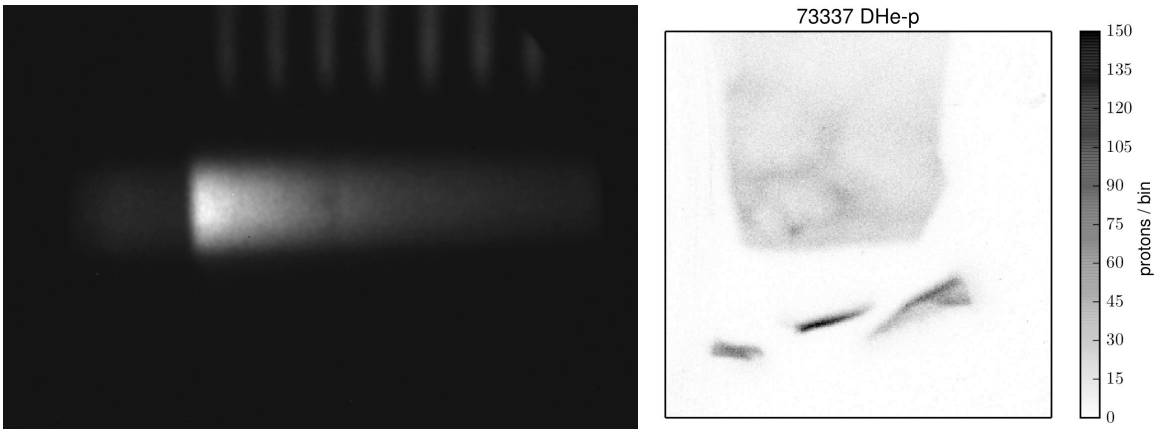

Figure E.13: Proton radiography data from 73337. Shot 73337 Particle Temporal Diagnostic (PTD) data on left; proton radiography on right. Data taken 30 ns after drive, 7 T field imposed.

E.9 73338

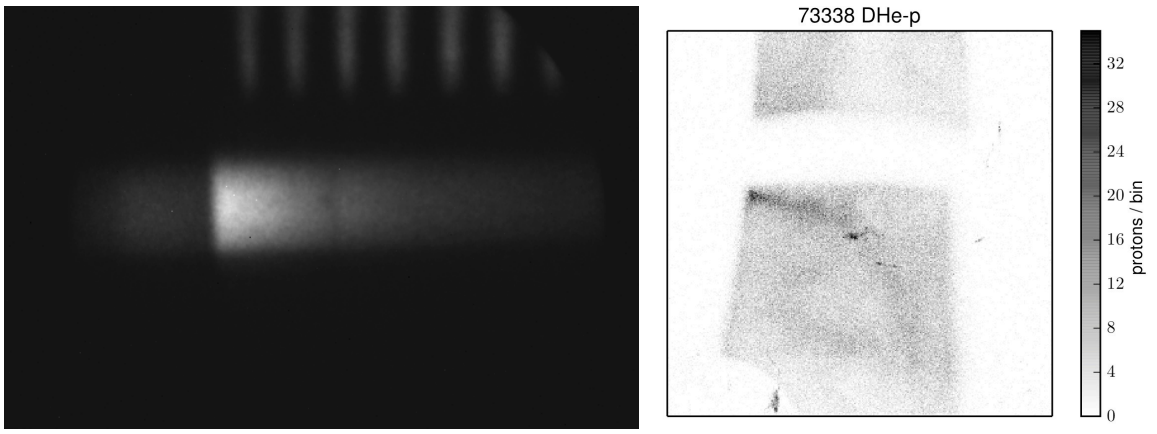

Figure E.14: Proton radiography data from 73338. Shot 73338 Particle Temporal Diagnostic (PTD) data on left; proton radiography on right. Data taken 50 ns after drive, 7 T field imposed.

E.10 73339

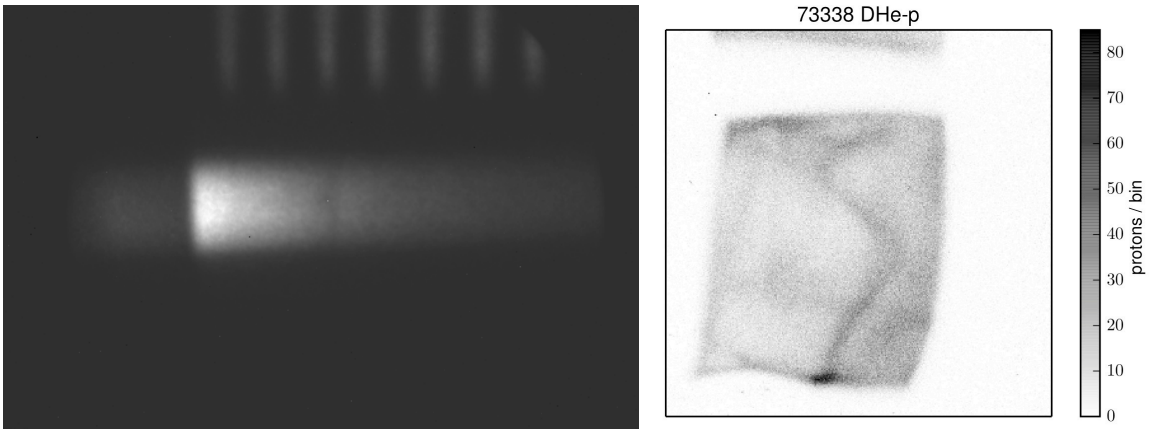

Figure E.15: Proton radiography data from 73339. Shot 73339 Particle Temporal Diagnostic (PTD) data on left; proton radiography on right. Data taken 30 ns after drive, 3 T field imposed.

E.11 73340

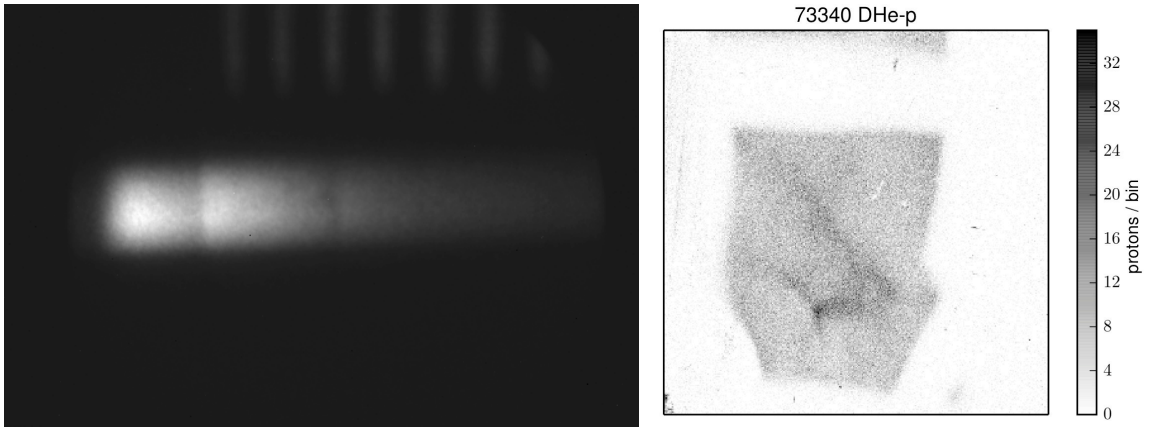

Figure E.16: Proton radiography data from 73340. Shot 73340 Particle Temporal Diagnostic (PTD) data on left; proton radiography on right. Data taken 50 ns after drive, 2.4 T field imposed.

E.12 73341

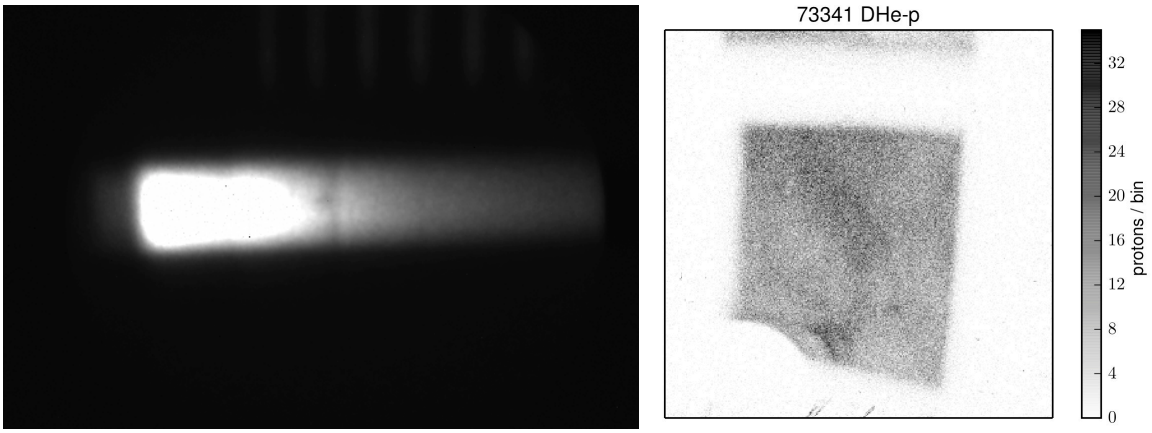

Figure E.17: Proton radiography data from 73341. Shot 73341 Particle Temporal Diagnostic (PTD) data on left; proton radiography on right. Data taken 70 ns after drive, 3 T field imposed.

E.13 73344

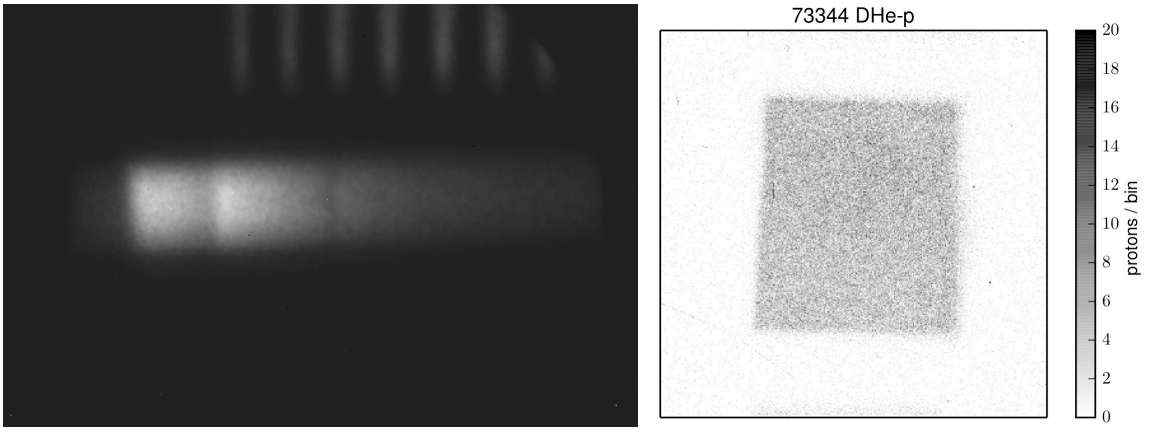

Figure E.18: Proton radiography data from 73344. Shot 73344 Particle Temporal Diagnostic (PTD) data on left; proton radiography on right. Data taken 70 ns after drive, field failed.

APPENDIX F

Data from May and October 2015

F.1 77250

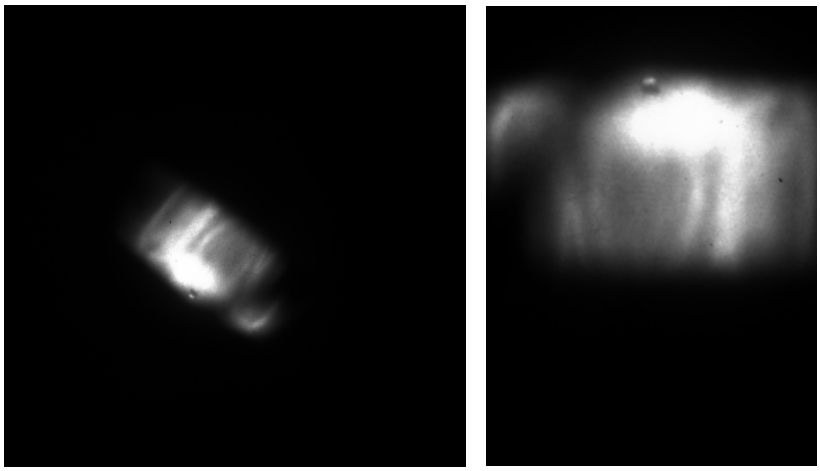

Figure F.1: Visible light data for 77250. Seven beam drive; images taken 23 ns later. This image used only an ND 2.0 filter, which resulted in damage to the camera. No proton radiography or magnetic field used on this shot. Left is the image from the CDD; right is the rotated, cropped image. This format will be used on all subsequent shots.

F.2 77251

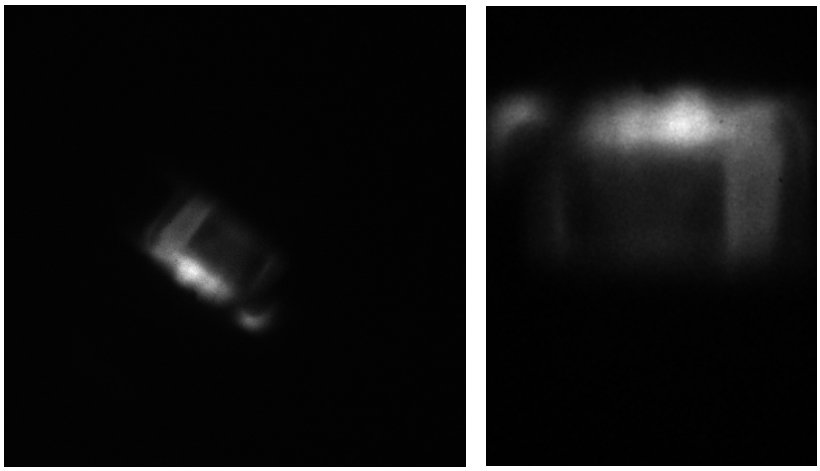

Figure F.2: Visible light data for 77251. Seven beam drive; images taken 13 ns later. Filtering was increased to ND 3.0+LP385 due to damage sustained during the previous shot (77250). No proton radiography or magnetic field used on this shot.

F.3 77254

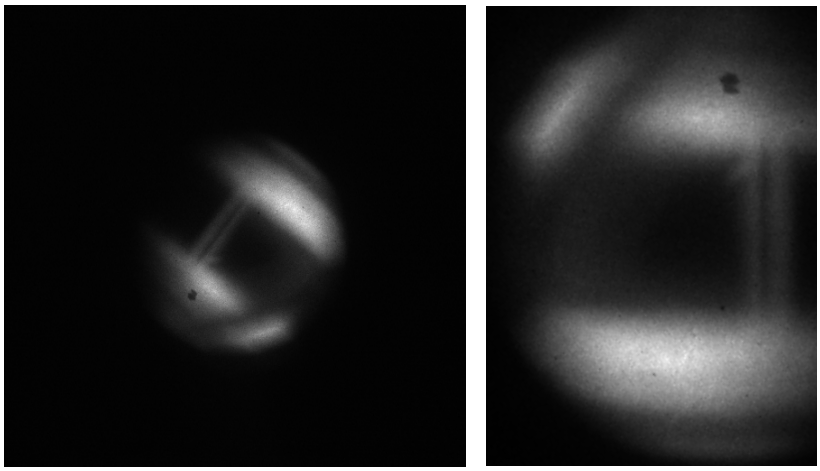

Figure F.3: Visible light data for 77254. A control shot; no jet was created but an 8 T magnetic field was imposed and proton radiography was used. In addition to the ND 3.0 and LP385 filters used previously, a VG380 was added. The dark splotch in the upper right of the cropped image is the damage to the CCD from earlier in the day. It is seen in all subsequent images.

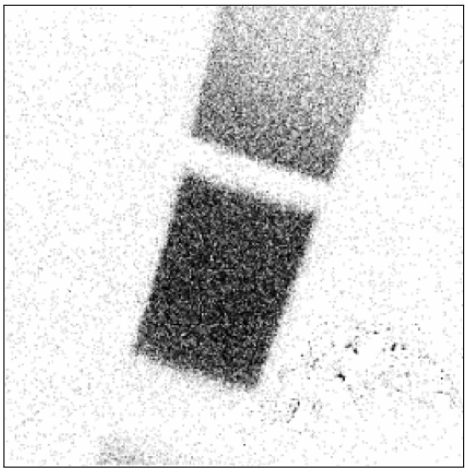

Figure F.4: Proton radiography data for 77254; 3 eV image failed (CR-39 frosted), 15 eV image shown above. Notice the fiducial notch is not visible in this image as it is in some of the others. We suspect this is because the MIFEDS coils "squeezed together" during the shot.

F.4 77255

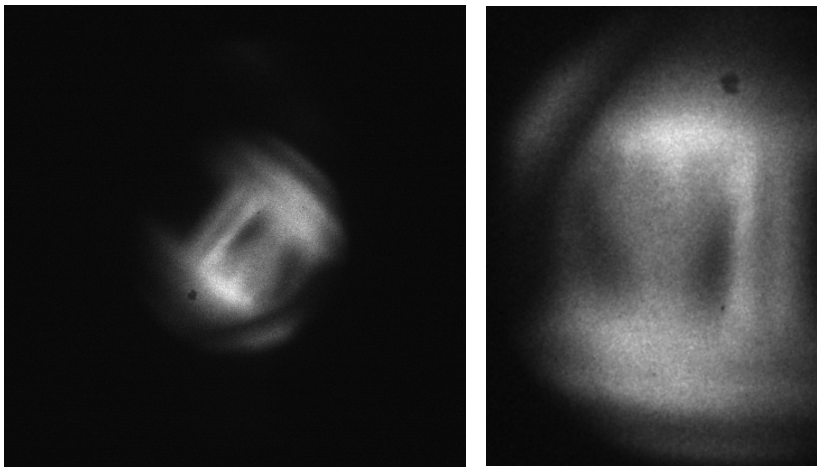

Figure F.5: Visible light data for 77255. Image was taken 13 ns after drive (one beam). An 8 T magnetic field was imposed and proton radiography was used. Filtering was unchanged from the previous shot (ND 3.0+LP385 +VG380).

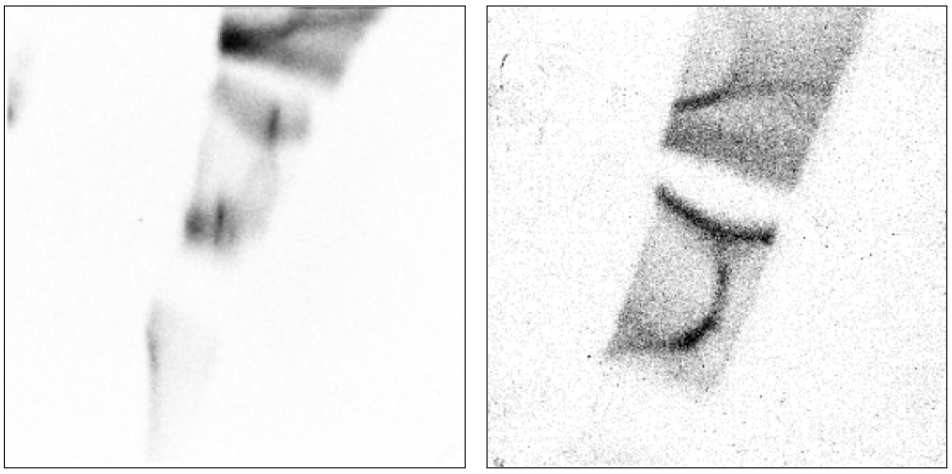

Figure F.6: Proton radiography data for 77255; 3 eV image left, 15 eV image right.

F.5 77256

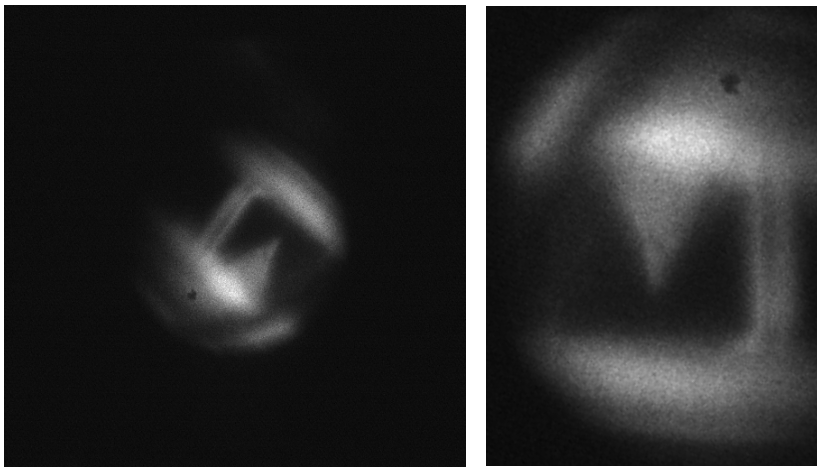

Figure F.7: Visible light data for 77256. Image was taken 23 ns after drive (one beam). An 8 T magnetic field was imposed and proton radiography was used. Filtering was unchanged from the previous shot (ND 3.0+LP385 +VG380).

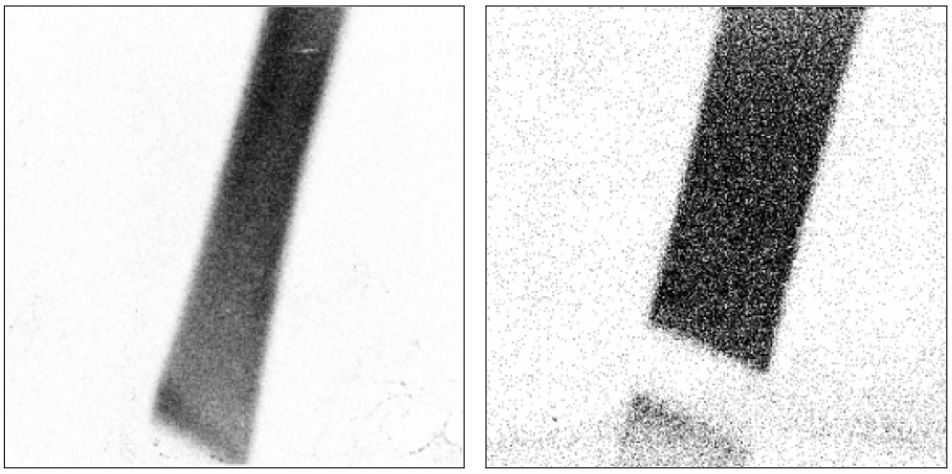

Figure F.8: Proton radiography data for 77256; 3 eV image left, 15 eV image right.

F.6 77258

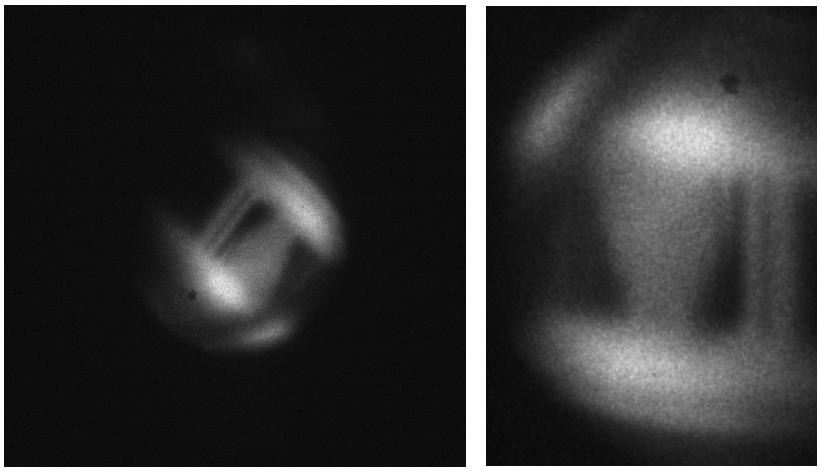

Figure F.9: Visible light data for 77258. Image was taken 43 ns after drive (one beam). An 8 T magnetic field was imposed and proton radiography was used. Filtering was unchanged from the previous shot (ND 3.0+LP385 +VG380).

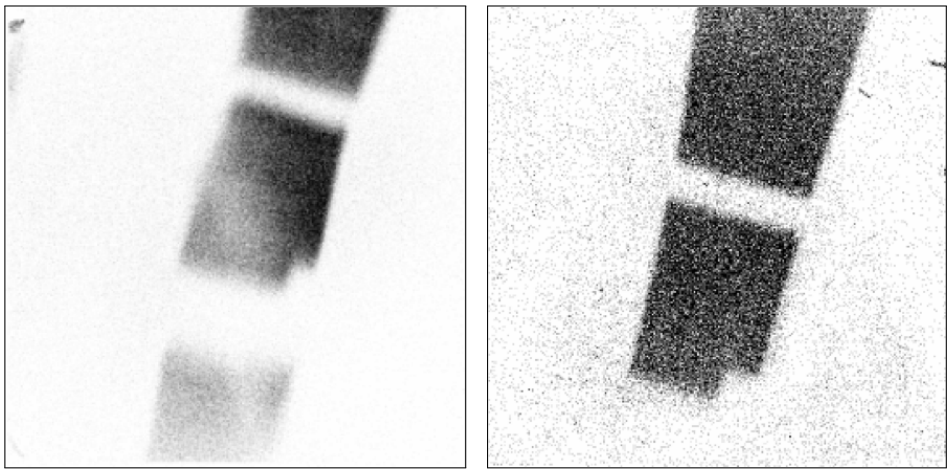

Figure F.10: Proton radiography data for 77258; 3 eV image left, 15 eV image right. In this pair of images, the fiducial notch is clearly visible.

F.7 77259

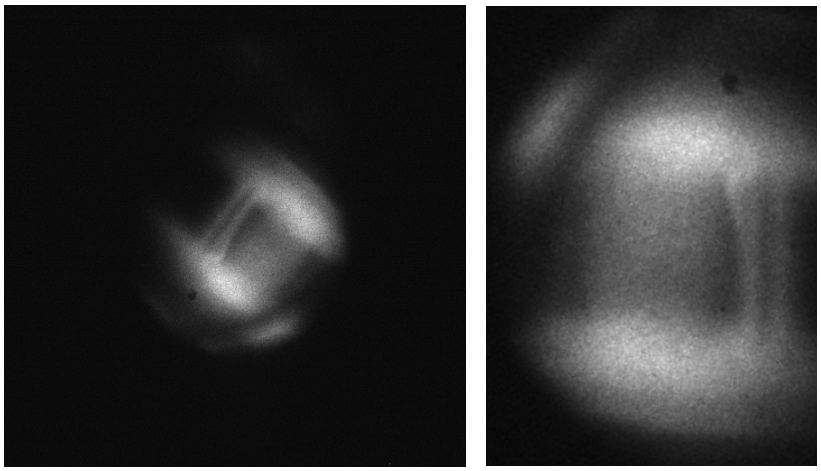

Figure F.11: Visible light data for 77259. Image was taken 63 ns after drive (one beam). An 8 T magnetic field was imposed and proton radiography was used. Filtering was unchanged from the previous shot (ND 3.0+LP385 +VG380).

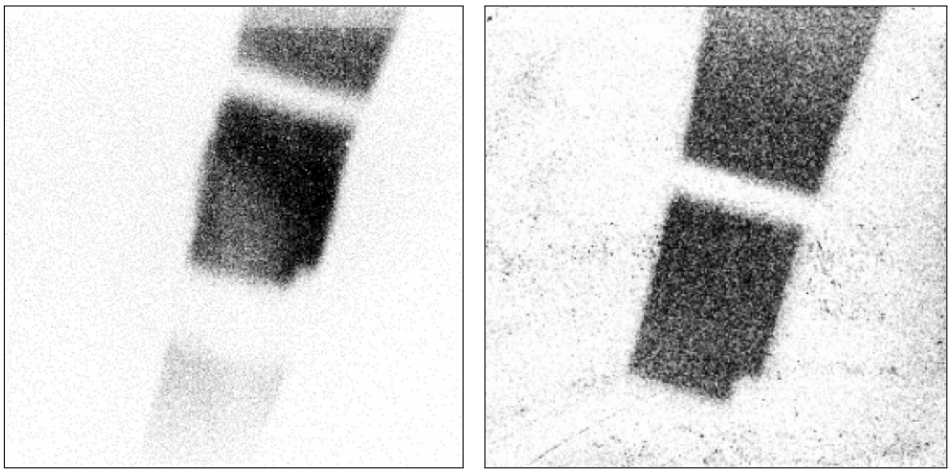

Figure F.12: Proton radiography data for 77259; 3 eV image left, 15 eV image right. Again, the fiducial notch is visible.

F.8 77260

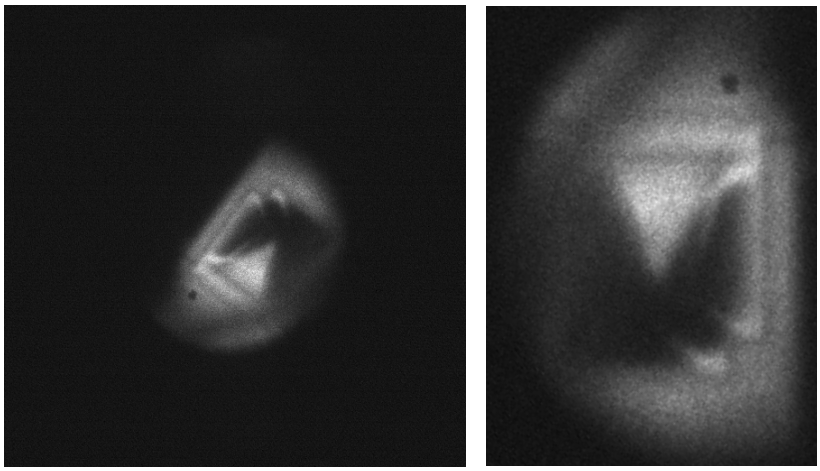

Figure F.13: Visible light data for 77260. Image was taken 23 ns after drive (one beam). No magnetic field was imposed and proton radiography was used. Filtering was unchanged from the previous shot (ND 3.0+LP385 +VG380). The fiducial notch is visible in these images; we hypothesize that it was not visible in previous images because the MIFEDS coils obscured it.

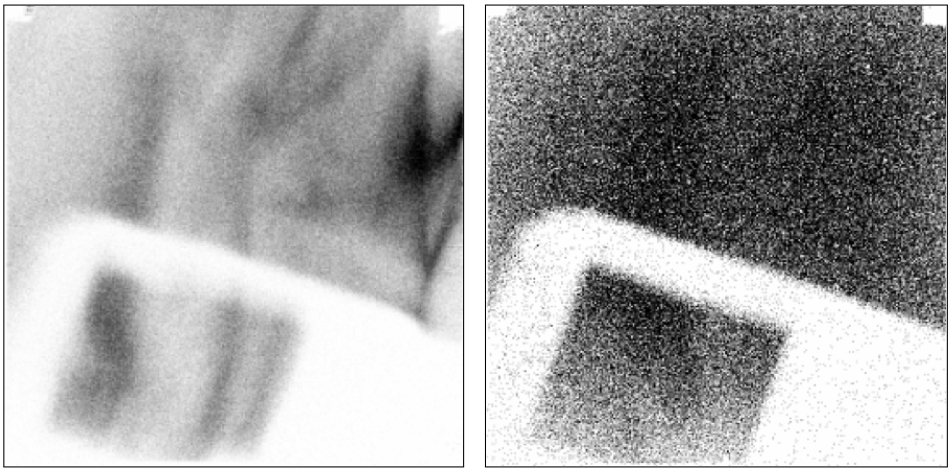

Figure F.14: Proton radiography data for 77260; 3 eV image left, 15 eV image right.

F.9 77261

Figure F.15: Visible light data for 77261. Image was taken 43 ns after drive (one beam). No magnetic field was imposed and proton radiography was used. Filtering was unchanged from the previous shot (ND 3.0+LP385 +VG380). This TPDI image failed, perhaps because it was timed to be ahead of the proton backlighter and could not make use of the reflected glow of the backlighter.

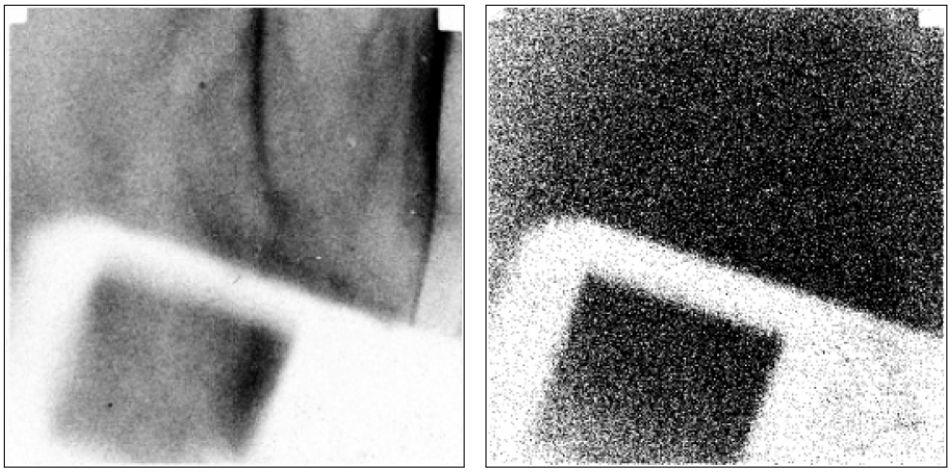

Figure F.16: Proton radiography data for 77261; 3 eV image left, 15 eV image right.

F.10 77262

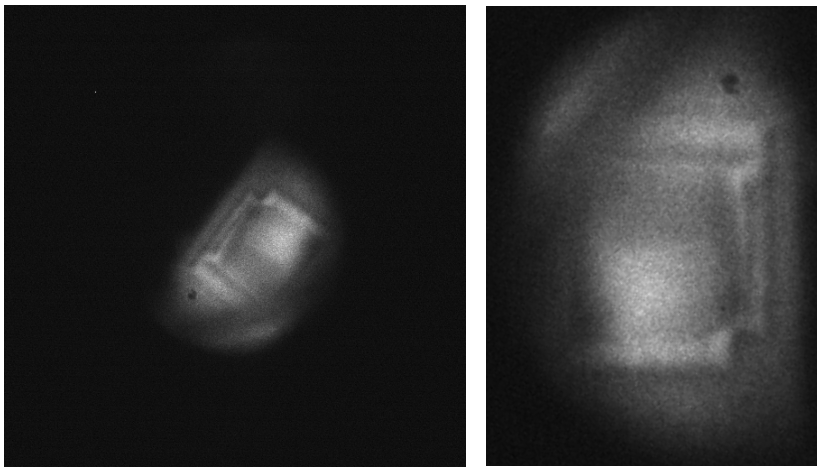

Figure F.17: Visible light data for 77262. Image was taken 63 ns after drive (one beam). No magnetic field was imposed and proton radiography was used. Filtering was unchanged from the previous shot (ND 3.0+LP385 +VG380). Again, the fiducial notch is visible.

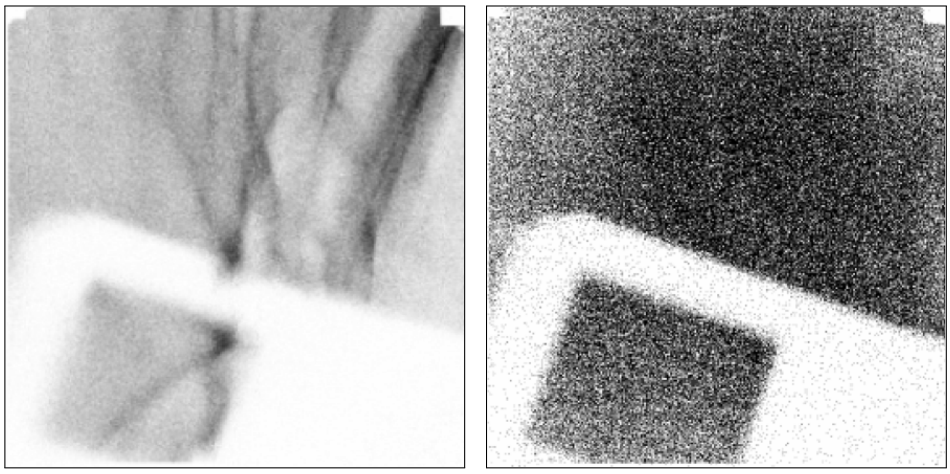

Figure F.18: Proton radiography data for 77262; 3 eV image left, 15 eV image right.

F.11 79221

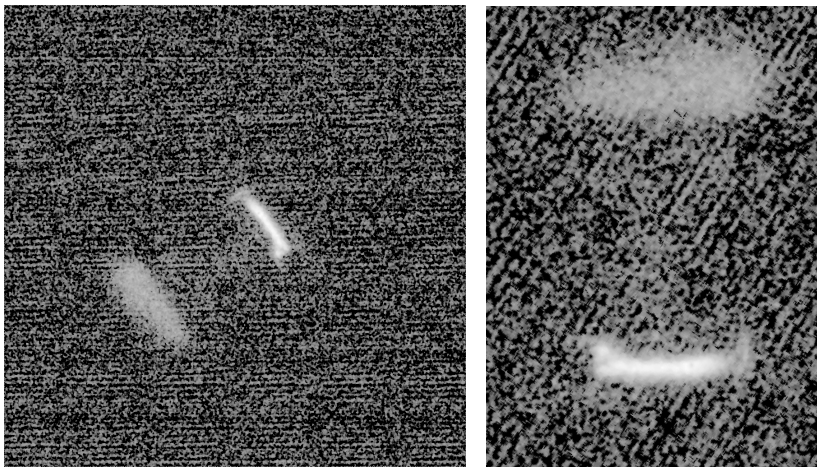

Figure F.19: Visible light data for 79221. Attempted re-do of Shot Shot 77261, the shot where TPDI failed in May 2015. Image was taken 43 ns after drive (one beam). No magnetic field was imposed and no proton radiography was used. Filtering was ND 2.0+LP385; image appears to be over-filtered.

F.12 79222

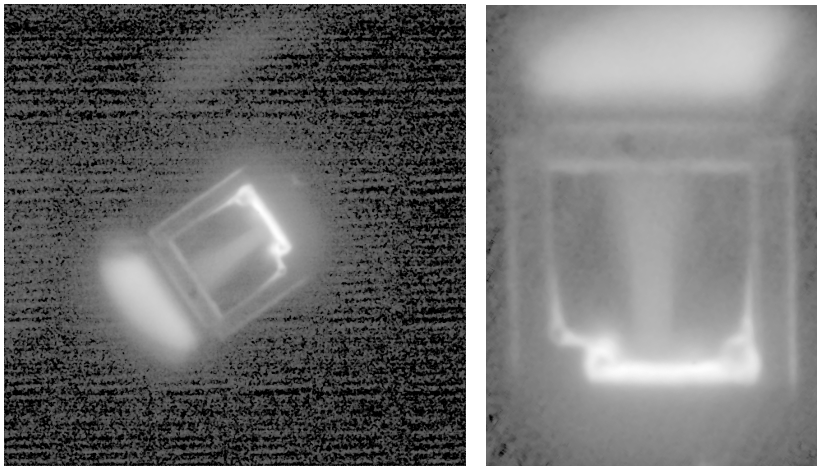

Figure F.20: Visible light data for 79222. Second attempted re-do of Shot Shot 77261. Image was taken 43 ns after drive (one beam). No magnetic field was imposed and no proton radiography was used. Filtering was reduced to LP385 (ND 2.0 was dropped).

BIBLIOGRAPHY

BIBLIOGRAPHY

Ardila, D. R., et al. (2013), Hot Gas Lines in T Tauri Stars, ApJS, *207*, 1, doi:10.1088/0067-0049/207/1/1.

Argiroffi, C., A. Maggio, and G. Peres (2007), X-ray emission from MP Muscae: an old classical T Tauri star, A&A, *465*, L5–L8, doi:10.1051/0004-6361:20067016.

Argiroffi, C., et al. (2011), Variable X-ray emission from the accretion shock in the classical T Tauri star V2129 Ophiuchi, A&A, *530*, A1, doi:10.1051/0004-6361/201016321.

Bellan, P. M. (2003), Why current-carrying magnetic flux tubes gobble up plasma and become thin as a result, *Physics of Plasmas*, *10*, 1999–2008, doi:10.1063/1.1558275.

Bellan, P. M. (2006), *Fundamentals of Plasma Physics*.

Bellan, P. M., et al. (2009), Astrophysical jets: Observations, numerical simulations, and laboratory experiments, *Physics of Plasmas*, *16*(4), 041,005–041,005, doi:10.1063/1.3101812.

Boehly, T. R., et al. (1997), Initial performance results of the OMEGA laser system, *Optics Communications*, *133*, 495–506, doi:10.1016/S0030-4018(96)00325-2.

Bouquet, S., E. Falize, C. Michaut, C. D. Gregory, B. Loupias, T. Vinci, and M. Koenig (2010), From lasers to the universe: Scaling laws in laboratory astrophysics, *High Energy Density Physics*, *6*, 368–380, doi:10.1016/j.hedp.2010.03.001.

Bouvier, J., S. H. P. Alencar, T. J. Harries, C. M. Johns-Krull, and M. M. Romanova (2007), Magnetospheric Accretion in Classical T Tauri Stars, *Protostars and Planets V*, pp. 479–494.

Brickhouse, N. S., S. R. Cranmer, A. K. Dupree, G. J. M. Luna, and S. Wolk (2010), A Deep Chandra X-Ray Spectrum of the Accreting Young Star TW Hydrae, ApJ, *710*, 1835–1847, doi:10.1088/0004-637X/710/2/1835.

Busschaert, C., É. Falize, B. Loupias, C. Michaut, A. Ravasio, A. Pelka, R. Yurchak, and M. Koenig (2013), POLAR project: a numerical study to optimize the target design, *New Journal of Physics*, *15*(3), 035020, doi:10.1088/1367-2630/15/3/035020.

Calvet, N., and E. Gullbring (1998), The Structure and Emission of the Accretion Shock in T Tauri Stars, ApJ, *509*, 802–818, doi:10.1086/306527.

Calvet, N., J. Muzerolle, C. Briceño, J. Hernández, L. Hartmann, J. L. Saucedo, and K. D. Gordon (2004), The Mass Accretion Rates of Intermediate-Mass T Tauri Stars, AJ, *128*, 1294–1318, doi:10.1086/422733.

Camenzind, M. (1990), Magnetized Disk-Winds and the Origin of Bipolar Outflows., in *Reviews in Modern Astronomy*, *Reviews in Modern Astronomy*, vol. 3, edited by G. Klare, pp. 234–265.

Chevalier, R. A., and J. N. Imamura (1982), Linear analysis of an oscillatory instability of radiative shock waves, ApJ, *261*, 543–549, doi:10.1086/160364.

Ciardi, A., S. V. Lebedev, A. Frank, F. Suzuki-Vidal, G. N. Hall, S. N. Bland, A. Harvey-Thompson, E. G. Blackman, and M. Camenzind (2009), Episodic Magnetic Bubbles and Jets: Astrophysical Implications from Laboratory Experiments, ApJ, *691*, L147–L150, doi:10.1088/0004-637X/691/2/L147.

Ciardi, A., et al. (2007), The evolution of magnetic tower jets in the laboratory, *Physics of Plasmas*, *14*(5), 056,501–056,501, doi:10.1063/1.2436479.

Coker, R. F., B. H. Wilde, J. M. Foster, B. E. Blue, P. A. Rosen, R. J. R. Williams, P. Hartigan, A. Frank, and C. A. Back (2007), Numerical Simulations and Astrophysical Applications of Laboratory Jets at Omega, Ap&SS, *307*, 57–62, doi:10.1007/s10509-006-9268-8.

Cross, J. E., et al. (2016), Laboratory analogue of a supersonic accretion column in a binary star system, *Nature Communications*, *7*, 11899, doi:10.1038/ncomms11899.

Donehew, B., and S. Brittain (2011), Measuring the Stellar Accretion Rates of Herbig Ae/Be Stars, AJ, *141*, 46, doi:10.1088/0004-6256/141/2/46.

Drake, J. J., J. Braithwaite, V. Kashyap, H. M. Günther, and N. J. Wright (2014), Burn Out or Fade Away? On the X-Ray and Magnetic Death of Intermediate Mass Stars, ApJ, *786*, 136, doi:10.1088/0004-637X/786/2/136.

Drake, R. P. (2006), *High-energy-density physics: fundamentals, inertial fusion, and experimental astrophysics*, xv, 534 p. pp., Springer, Berlin ; New York.

Drake, R. P. (2011), Isothermal, mass-limited rarefactions in planar and spherical geometry, *Physics of Plasmas*, *18*(10), 104506, doi:10.1063/1.3642612.

Dullemond, C. P., C. Dominik, and A. Natta (2001), Passive Irradiated Circumstellar Disks with an Inner Hole, ApJ, *560*, 957–969, doi:10.1086/323057.

Edwards, S., P. Hartigan, L. Ghandour, and C. Andrulis (1994), Spectroscopic evidence for magnetospheric accretion in classical T Tauri stars, AJ, *108*, doi:10.1086/117134.

Eliezer, S. (2002), The Interaction of High-Power Lasers with Plasmas, *The Interaction of High-Power Lasers with Plasmas. Series: Series in Plasma Physics, ISBN: ¡ISBN¿978-0-7503-0747-5¡/ISBN¿. Taylor Francis, Edited by Shalom Eliezer, vol. 11*, *11*, doi:10.1201/9781420033380.

Falize, É., A. Ravasio, B. Loupias, A. Dizière, C. D. Gregory, C. Michaut, C. Busschaert, C. Cavet, and M. Koenig (2012), High-energy density laboratory astrophysics studies of accretion shocks in magnetic cataclysmic variables, *High Energy Density Physics*, *8*, 1–4, doi:10.1016/j.hedp.2011.10.001.

Farley, D. R., et al. (1999), Radiative Jet Experiments of Astrophysical Interest Using Intense Lasers, *Physical Review Letters*, *83*, 1982–1985, doi:10.1103/PhysRevLett.83.1982.

Fiksel, G., W. Fox, A. Bhattacharjee, D. H. Barnak, P.-Y. Chang, K. Germaschewski, S. X. Hu, and P. M. Nilson (2014), Magnetic Reconnection between Colliding Magnetized Laser-Produced Plasma Plumes, *Physical Review Letters*, *113*(10), 105003, doi:10.1103/PhysRevLett.113.105003.

Fiksel, G., et al. (2015), Note: Experimental platform for magnetized high-energy-density plasma studies at the omega laser facility, *Review of Scientific Instruments*, *86*(1), 016105, doi:10.1063/1.4905625.

Foster, J. M., et al. (2005), High-Energy-Density Laboratory Astrophysics Studies of Jets and Bow Shocks, ApJ, *634*, L77–L80, doi:10.1086/498846.

Fox, W., G. Fiksel, A. Bhattacharjee, P.-Y. Chang, K. Germaschewski, S. X. Hu, and P. M. Nilson (2013), Filamentation Instability of Counterstreaming Laser-Driven Plasmas, *Physical Review Letters*, *111*(22), 225002, doi:10.1103/PhysRevLett.111.225002.

Froula, D. H., S. H. Glenzer, N. C. Luhmann, and J. Sheffield (2011), *Plasma scattering of electromagnetic radiation: theory and measurement techniques*, 2 ed., Academic Press/Elsevier, Burlington, MA.

Garcia Lopez, R., A. Natta, L. Testi, and E. Habart (2006), Accretion rates in Herbig Ae stars, A&A, *459*, 837–842, doi:10.1051/0004-6361:20065575.

Ghosh, P., and F. K. Lamb (1979a), Accretion by rotating magnetic neutron stars. II - Radial and vertical structure of the transition zone in disk accretion, ApJ, *232*, 259–276, doi:10.1086/157285.

Ghosh, P., and F. K. Lamb (1979b), Accretion by rotating magnetic neutron stars. III - Accretion torques and period changes in pulsating X-ray sources, ApJ, *234*, 296–316, doi:10.1086/157498.

Gotchev, O. V., J. P. Knauer, P. Y. Chang, N. W. Jang, M. J. Shoup, D. D. Meyerhofer, and R. Betti (2009), Seeding magnetic fields for laser-driven flux compression

in high-energy-density plasmas, *Review of Scientific Instruments*, *80*(4), 043,504–043,504, doi:10.1063/1.3115983.

Grady, C. A., et al. (2010), Locating the Accretion Footprint on a Herbig Ae Star: MWC 480, ApJ, *719*, 1565–1581, doi:10.1088/0004-637X/719/2/1565.

Gregory, C. D., et al. (2008), Astrophysical Jet Experiments with Colliding Laser-produced Plasmas, ApJ, *676*, 420–426, doi:10.1086/527352.

Gregory, C. D., et al. (2010), Laser-driven plasma jets propagating in an ambient gas studied with optical and proton diagnostics, *Physics of Plasmas*, *17*(5), 052708, doi:10.1063/1.3431094.

Grinin, V. P., O. V. Kozlova, A. Natta, I. Ilyin, I. Tuominen, A. N. Rostopchina, and D. N. Shakhovskoy (2001), Optical spectra of five UX Orionis-type stars, A&A, *379*, 482–495, doi:10.1051/0004-6361:20011280.

Günther, H. M., C. Liefke, J. H. M. M. Schmitt, J. Robrade, and J.-U. Ness (2006), X-ray accretion signatures in the close CTTS binary V4046 Sagittarii, A&A, *459*, L29–L32, doi:10.1051/0004-6361:20066306.

Hartigan, P., S. J. Kenyon, L. Hartmann, S. E. Strom, S. Edwards, A. D. Welty, and J. Stauffer (1991), Optical excess emission in T Tauri stars, ApJ, *382*, 617–635, doi:10.1086/170749.

Hartigan, P., A. Frank, J. M. Foster, B. H. Wilde, M. Douglas, P. A. Rosen, R. F. Coker, B. E. Blue, and J. F. Hansen (2011), Fluid Dynamics of Stellar Jets in Real Time: Third Epoch Hubble Space Telescope Images of HH 1, HH 34, and HH 47, ApJ, *736*, 29, doi:10.1088/0004-637X/736/1/29.

Hartigan, P., et al. (2009), Laboratory Experiments, Numerical Simulations, and Astronomical Observations of Deflected Supersonic Jets: Application to HH 110, ApJ, *705*, 1073–1094, doi:10.1088/0004-637X/705/1/1073.

Hartmann, L., N. Calvet, E. Gullbring, and P. D'Alessio (1998), Accretion and the Evolution of T Tauri Disks, ApJ, *495*, 385, doi:10.1086/305277.

Herbig, G. H. (1960), The Spectra of Be- and Ae-TYPE Stars Associated with Nebulosity, ApJS, *4*, 337, doi:10.1086/190050.

Herbig, G. H. (1962), The properties and problems of T Tauri stars and related objects., *Advances in Astronomy and Astrophysics*, *1*, 47–103.

Hillenbrand, L. A., S. E. Strom, F. J. Vrba, and J. Keene (1992), Herbig Ae/Be stars - Intermediate-mass stars surrounded by massive circumstellar accretion disks, ApJ, *397*, 613–643, doi:10.1086/171819.

Hohenberger, M., et al. (2010), Observation of a Velocity Domain Cooling Instability in a Radiative Shock, *Physical Review Letters*, *105*(20), 205003, doi:10.1103/PhysRevLett.105.205003.

Huba, J. D., U. States., and N. R. L. U. S.) (2009), *NRL plasma formulary*, 1 online resource [71 p.] pp., Naval Research Laboratory], [Washington, DC.

Hubrig, S., M. Schöller, and R. V. Yudin (2004), Magnetic fields in Herbig Ae stars, A&A, *428*, L1–L4, doi:10.1051/0004-6361:200400091.

Hubrig, S., R. V. Yudin, M. Schöller, and M. A. Pogodin (2006), Accurate magnetic field measurements of Vega-like stars and Herbig Ae/Be stars, A&A, *446*, 1089–1094, doi:10.1051/0004-6361:20053794.

Ingleby, L., et al. (2013), Accretion Rates for T Tauri Stars Using Nearly Simultaneous Ultraviolet and Optical Spectra, ApJ, *767*, 112, doi:10.1088/0004-637X/767/2/112.

Ji, H., M. Burin, E. Schartman, and J. Goodman (2006), Hydrodynamic turbulence cannot transport angular momentum effectively in astrophysical disks, Nature, *444*, 343–346, doi:10.1038/nature05323.

Johns-Krull, C. M. (2007), The Magnetic Fields of Classical T Tauri Stars, ApJ, *664*, 975–985, doi:10.1086/519017.

Johns-Krull, C. M., J. A. Valenti, and C. Koresko (1999), Measuring the Magnetic Field on the Classical T Tauri Star BP Tauri, ApJ, *516*, 900–915, doi:10.1086/307128.

Joy, A. H. (1945), T Tauri Variable Stars., ApJ, *102*, 168, doi:10.1086/144749.

Kastner, J. H., D. P. Huenemoerder, N. S. Schulz, C. R. Canizares, and D. A. Weintraub (2002), Evidence for Accretion: High-Resolution X-Ray Spectroscopy of the Classical T Tauri Star TW Hydrae, ApJ, *567*, 434–440, doi:10.1086/338419.

Katz, J., R. Boni, C. Sorce, R. Follett, M. J. Shoup, and D. H. Froula (2012), A reflective optical transport system for ultraviolet Thomson scattering from electron plasma waves on OMEGAa), *Review of Scientific Instruments*, *83*(10), 10E349–10E349, doi:10.1063/1.4733551.

Katz, J., J. S. Ross, C. Sorce, and D. H. Froula (2013), A reflective image-rotating periscope for spatially resolved Thomson-scattering experiments on OMEGA, *Journal of Instrumentation*, *8*, C12009, doi:10.1088/1748-0221/8/12/C12009.

Knauer, J. P., et al. (2010), Compressing magnetic fields with high-energy lasersa), *Physics of Plasmas*, *17*(5), 056318, doi:10.1063/1.3416557.

Koenigl, A. (1991), Disk accretion onto magnetic T Tauri stars, ApJ, *370*, L39–L43, doi:10.1086/185972.

Krauland, C. M., et al. (2013), Reverse Radiative Shock Laser Experiments Relevant to Accreting Stream-Disk Impact in Interacting Binaries, ApJ, *762*, L2, doi:10.1088/2041-8205/762/1/L2.

Kuranz, C. C., et al. (2009), Two-Dimensional Blast-Wave-Driven Rayleigh-Taylor Instability: Experiment and Simulation, ApJ, *696*, 749–759, doi:10.1088/0004-637X/696/1/749.

Lebedev, S. V., D. Ampleford, A. Ciardi, S. N. Bland, J. P. Chittenden, M. G. Haines, A. Frank, E. G. Blackman, and A. Cunningham (2004), Jet Deflection via Cross-winds: Laboratory Astrophysical Studies, ApJ, *616*, 988–997, doi:10.1086/423730.

Lebedev, S. V., et al. (2002), Laboratory Astrophysics and Collimated Stellar Outflows: The Production of Radiatively Cooled Hypersonic Plasma Jets, ApJ, *564*, 113–119, doi:10.1086/324183.

Lebedev, S. V., et al. (2005a), Magnetic tower outflows from a radial wire array Z-pinch, MNRAS, *361*, 97–108, doi:10.1111/j.1365-2966.2005.09132.x.

Lebedev, S. V., et al. (2005b), Production of radiatively cooled hypersonic plasma jets and links to astrophysical jets, *Plasma Physics and Controlled Fusion*, *47*, B465–B479, doi:10.1088/0741-3335/47/12B/S33.

Li, C. K., F. H. Séguin, J. A. Frenje, J. R. Rygg, R. D. Petrasso, R. P. J. Town, O. L. Landen, J. P. Knauer, and V. A. Smalyuk (2007), Observation of Megagauss-Field Topology Changes due to Magnetic Reconnection in Laser-Produced Plasmas, *Physical Review Letters*, *99*(5), 055001, doi:10.1103/PhysRevLett.99.055001.

Li, C. K., et al. (2006), Measuring E and B Fields in Laser-Produced Plasmas with Monoenergetic Proton Radiography, *Physical Review Letters*, *97*(13), 135003, doi:10.1103/PhysRevLett.97.135003.

Li, C. K., et al. (2013), Structure and Dynamics of Colliding Plasma Jets, *Physical Review Letters*, *111*(23), 235003, doi:10.1103/PhysRevLett.111.235003.

Loupias, B., et al. (2007), Supersonic-Jet Experiments Using a High-Energy Laser, *Physical Review Letters*, *99*(26), 265001, doi:10.1103/PhysRevLett.99.265001.

Loupias, B., et al. (2009), Experimental results to study astrophysical plasma jets using Intense Lasers, Ap&SS, *322*, 25–29, doi:10.1007/s10509-009-0025-7.

Mendigutía, I., N. Calvet, B. Montesinos, A. Mora, J. Muzerolle, C. Eiroa, R. D. Oudmaijer, and B. Merín (2011), Accretion rates and accretion tracers of Herbig Ae/Be stars, A&A, *535*, A99, doi:10.1051/0004-6361/201117444.

Moser, A. L., and P. M. Bellan (2012), Observations of magnetic flux compression in jet impact experiments, Ap&SS, *337*, 593–596, doi:10.1007/s10509-011-0860-1.

Muzerolle, J., L. Hartmann, and N. Calvet (1998), A Brgamma Probe of Disk Accretion in T Tauri Stars and Embedded Young Stellar Objects, AJ, *116*, 2965–2974, doi:10.1086/300636.

Muzerolle, J., P. D'Alessio, N. Calvet, and L. Hartmann (2004), Magnetospheres and Disk Accretion in Herbig Ae/Be Stars, ApJ, *617*, 406–417, doi:10.1086/425260.

Muzerolle, J., K. L. Luhman, C. Briceño, L. Hartmann, and N. Calvet (2005), Measuring Accretion in Young Substellar Objects: Approaching the Planetary Mass Regime, ApJ, *625*, 906–912, doi:10.1086/429483.

Natta, A., V. P. Grinin, and L. V. Tambovtseva (2000), An Interesting Episode of Accretion Activity in UX Orionis, ApJ, *542*, 421–427, doi:10.1086/309526.

Natta, A., T. Prusti, R. Neri, D. Wooden, V. P. Grinin, and V. Mannings (2001), A reconsideration of disk properties in Herbig Ae stars, A&A, *371*, 186–197, doi:10.1051/0004-6361:20010334.

Natta, A., L. Testi, and S. Randich (2006), Accretion in the ρ-Ophiuchi pre-main sequence stars, A&A, *452*, 245–252, doi:10.1051/0004-6361:20054706.

Orlando, S., G. G. Sacco, C. Argiroffi, F. Reale, G. Peres, and A. Maggio (2010), X-ray emitting MHD accretion shocks in classical T Tauri stars. Case for moderate to high plasma-β values, A&A, *510*, A71, doi:10.1051/0004-6361/200913565.

Remington, B. A., R. P. Drake, H. Takabe, and D. Arnett (2000), A review of astrophysics experiments on intense lasers, *Physics of Plasmas*, *7*, 1641–1652, doi:10.1063/1.874046.

Remington, B. A., R. P. Drake, and D. D. Ryutov (2006), Experimental astrophysics with high power lasers and Z pinches, *Reviews of Modern Physics*, *78*, 755–807, doi:10.1103/RevModPhys.78.755.

Robrade, J., and J. H. M. M. Schmitt (2007), X-rays from RU Lupi: accretion and winds in classical T Tauri stars, A&A, *473*, 229–238, doi:10.1051/0004-6361:20077644.

Romanova, M. M., G. V. Ustyugova, A. V. Koldoba, and R. V. E. Lovelace (2004), Three-dimensional Simulations of Disk Accretion to an Inclined Dipole. II. Hot Spots and Variability, ApJ, *610*, 920–932, doi:10.1086/421867.

Ross, J. S., et al. (2012), Characterizing counter-streaming interpenetrating plasmas relevant to astrophysical collisionless shocks, *Physics of Plasmas*, *19*(5), 056,501, doi:10.1063/1.3694124.

Ryutov, D., R. P. Drake, J. Kane, E. Liang, B. A. Remington, and W. M. Wood-Vasey (1999), Similarity Criteria for the Laboratory Simulation of Supernova Hydrodynamics, ApJ, *518*, 821–832, doi:10.1086/307293.

Ryutov, D. D. (2011), Using intense lasers to simulate aspects of accretion discs and outflows in astrophysics, Ap&SS, *336*, 21–26, doi:10.1007/s10509-010-0558-9.

Schmitt, J. H. M. M., J. Robrade, J.-U. Ness, F. Favata, and B. Stelzer (2005), X-rays from accretion shocks in T Tauri stars: The case of BP Tau, A&A, *432*, L35–L38, doi:10.1051/0004-6361:200500014.

Séguin, F. H., et al. (2003), Spectrometry of charged particles from inertial-confinement-fusion plasmas, *Review of Scientific Instruments*, *74*, 975–995, doi:10.1063/1.1518141.

Shigemori, K., et al. (2000), Experiments on radiative collapse in laser-produced plasmas relevant to astrophysical jets, Phys. Rev. E, *62*, 8838–8841, doi:10.1103/PhysRevE.62.8838.

Sisan, D. R., N. Mujica, W. A. Tillotson, Y.-M. Huang, W. Dorland, A. B. Hassam, T. M. Antonsen, and D. P. Lathrop (2004), Experimental Observation and Characterization of the Magnetorotational Instability, *Physical Review Letters*, *93*(11), 114502, doi:10.1103/PhysRevLett.93.114502.

Soures, J. M., et al. (1996), Direct-drive laser-fusion experiments with the OMEGA, 60-beam, $>$ 40 kJ, ultraviolet laser system, *Physics of Plasmas*, *3*, 2108–2112, doi:10.1063/1.871662.

Stefani, F., T. Gundrum, G. Gerbeth, G. Rüdiger, M. Schultz, J. Szklarski, and R. Hollerbach (2006), Experimental Evidence for Magnetorotational Instability in a Taylor-Couette Flow under the Influence of a Helical Magnetic Field, *Physical Review Letters*, *97*(18), 184502, doi:10.1103/PhysRevLett.97.184502.

Stelzer, B., and J. H. M. M. Schmitt (2004), X-ray emission from a metal depleted accretion shock onto the classical T Tauri star TW Hya, A&A, *418*, 687–697, doi:10.1051/0004-6361:20040041.

Suzuki-Vidal, F., et al. (2010), Generation of episodic magnetically driven plasma jets in a radial foil Z-pinch, *Physics of Plasmas*, *17*(11), 112,708–112,708, doi:10.1063/1.3504221.

Swartz, D. A., J. J. Drake, R. F. Elsner, K. K. Ghosh, C. A. Grady, E. Wassell, B. E. Woodgate, and R. A. Kimble (2005), The Herbig Ae Star HD 163296 in X-Rays, ApJ, *628*, 811–816, doi:10.1086/429984.

Testa, P., D. P. Huenemoerder, N. S. Schulz, and K. Ishibashi (2008), X-Ray Emission from Young Stellar Objects in the ϵ Chamaeleontis Group: The Herbig Ae Star HD 104237 and Associated Low-Mass Stars, ApJ, *687*, 579–597, doi:10.1086/591485.

Valenti, J. A., and C. M. Johns-Krull (2004), Observations of Magnetic Fields on T Tauri Stars, Ap&SS, *292*, 619–629, doi:10.1023/B:ASTR.0000045068.34836.cf.

Valenti, J. A., G. Basri, and C. M. Johns (1993), T Tauri stars in blue, AJ, *106*, 2024–2050, doi:10.1086/116783.

Wade, G. A., S. Bagnulo, D. Drouin, J. D. Landstreet, and D. Monin (2007), A search for strong, ordered magnetic fields in Herbig Ae/Be stars, MNRAS, *376*, 1145–1161, doi:10.1111/j.1365-2966.2007.11495.x.

Yang, H., C. M. Johns-Krull, and J. A. Valenti (2005), Measuring the Magnetic Field of the Classical T Tauri Star TW Hydrae, ApJ, *635*, 466–475, doi:10.1086/497070.

You, S., G. S. Yun, and P. M. Bellan (2005), Dynamic and Stagnating Plasma Flow Leading to Magnetic-Flux-Tube Collimation, *Physical Review Letters*, *95*(4), 045002, doi:10.1103/PhysRevLett.95.045002.

Yun, G. S., and P. M. Bellan (2010), Plasma tubes becoming collimated as a result of magnetohydrodynamic pumping, *Physics of Plasmas*, *17*(6), 062,108–062,108, doi:10.1063/1.3437075.